European Journal of Medicinal Chemistry 286 (2025) 117265

Contents lists available at ScienceDirect

European Journal of Medicinal Chemistry

journal homepage: www.elsevier.com/locate/ejmech

Research paper

[^{18}F]R91150: Improved radiosynthesis and in vivo evaluation as imaging probe for 5-HT$_{2A}$ receptors

Chris Hoffmann [a,b], Heike Endepols [a,b,c], Elizaveta A. Urusova [a,b], Dominik Elchine [a], Felix Neumaier [a,b], Bernd Neumaier [a,b,*], Boris D. Zlatopolskiy [a,b]

[a] Forschungszentrum Jülich GmbH, Institute of Neuroscience and Medicine, Nuclear Chemistry (INM-5), Wilhelm-Johnen-Straße, 52428, Jülich, Germany
[b] University of Cologne, Faculty of Medicine and University Hospital Cologne, Institute of Radiochemistry and Experimental Molecular Imaging, Kerpener Straße 62, 50937, Cologne, Germany
[c] University of Cologne, Faculty of Medicine and University Hospital Cologne, Department of Nuclear Medicine, Kerpener Straße 62, 50937, Cologne, Germany

ARTICLE INFO

Keywords:
5-HT$_{2A}$ receptors
Copper-mediated radiofluorination
Fluorine-18
Positron emission tomography
Radiopharmaceuticals
Imaging agents

ABSTRACT

Serotonergic 5-HT$_{2A}$ receptors in the cortex and other forebrain structures have been linked to cognitive, emotional and memory processes. In addition, dysfunction or altered expression of these receptors is associated with neuropsychiatric and neurodegenerative disorders. [^{18}F]R91150 is a candidate radiotracer for positron emission tomography (PET) imaging of 5-HT$_{2A}$ receptors, which showed promising properties in *in vitro* studies. However, existing methods for the production of [^{18}F]R91150 are rather inefficient and its imaging properties have not been studied *in vivo*. In the present work, we describe improved protocols for preparation of [^{18}F]R91150, the corresponding reference compound and two alternative boronate radiolabeling precursors. Furthermore, we present the results of an *in vivo* evaluation of the radioligand in rodents. [^{18}F]R91150 was prepared in activity yields of 20 ± 5% (two-step radiosynthesis) or 12 ± 2% (one-step radiosynthesis) and with molar activities of >200 GBq/μmol. μPET measurements in mice revealed sufficient stability against *in vivo* defluorination and predominantly hepatobiliary excretion of the tracer, with high radioactivity uptake in gall bladder and intestines. μPET imaging in rats demonstrated specific tracer accumulation in the cortex and subcortical forebrain structures, which could be reduced by pretreatment or displacement with the 5-HT$_{2A}$ receptor ligands altanserin or ketanserin but was insensitive to pretreatment with the 5-HT$_{2C}$ receptor ligand SB242084. In addition, [^{18}F]R91150 showed specific accumulation in the choroid plexus that was much less sensitive to displacement with ketanserin and unaffected by pretreatment with altanserin or SB242084. Taken together, our results indicate that [^{18}F]R91150 may be a promising candidate for *in vivo* PET imaging of cortical 5-HT$_{2A}$ receptors, although further studies will be required to elucidate the mechanisms underlying tracer accumulation in the choroid plexus.

1. Introduction

The serotonergic 5-HT$_{2A}$ receptor system in the cortex and other forebrain structures is involved in the effects of serotonin (5-HT) on various cognitive, emotional, and memory processes [1–3]. It has also been implicated in the pathogenesis of neuropsychiatric and neurodegenerative diseases [4–7]. For example, a profound reduction of cortical 5-HT$_{2A}$ receptor densities that typically correlates with the severity of cognitive decline has consistently been detected in patients with Alzheimer's disease [8–11]. Conversely, several imaging studies found an increased availability of 5-HT$_{2A}$ receptors in the cortex of patients with major depression characterized by high levels of dysfunctional attitudes [12,13]. Accordingly, 5-HT$_{2A}$ receptor antagonists have been proposed as promising therapeutic agents for depression and other affective disorders like schizophrenia or anxiety disorders [14–16]. However, the exact functional relevance of 5-HT$_{2A}$ receptors in diseases like schizophrenia remains controversial, as studies of their expression and/or availability in affected patients have reported contradictory results [17–21]. Methods to visualize 5-HT$_{2A}$ receptors and their interaction with drug candidates are crucial for further studies on their

* Corresponding author. Forschungszentrum Jülich GmbH, Institute of Neuroscience and Medicine, Nuclear Chemistry (INM-5), Wilhelm-Johnen-Straße, 52428, Jülich, Germany.
E-mail address: b.neumaier@fz-juelich.de (B. Neumaier).

https://doi.org/10.1016/j.ejmech.2025.117265
Received 23 August 2024; Received in revised form 22 November 2024; Accepted 7 January 2025
Available online 9 January 2025

pathophysiological significance as well as for the development of appropriate therapeutic approaches. Nuclear medicine techniques such as positron emission tomography (PET) or single photon emission computed tomography (SPECT) are particularly well suited for this purpose, as they enable non-invasive molecular imaging in living subjects. Accordingly, several 5-HT_{2A} receptor antagonists labeled with positron-emitting radionuclides, such as [^{18}F]altanserin [22–25], [^{18}F]setoperone [26–29] or [^{11}C]MDL100907 [13,30,31] (Fig. 1A), have been developed and used for preclinical and clinical PET studies. However, their practical utility is limited by the formation of brain-penetrating radiometabolites (e.g., [^{18}F]altanserin [32]), off-target binding (e.g., [^{18}F]altanserin and [^{18}F]setoperone [26,33,34]) or the short half-life of carbon-11 (e.g., [^{11}C]MDL100907 [30]). One approach to overcome these issues has been the development of [^{18}F]MDL100907 [35–37] or other ^{18}F-labeled tracers based on the MDL100907 scaffold like *R*-[^{18}F]MH.MZ [38,39], which combine the favorable binding profile of [^{11}C]MDL100907 with the superior isotopic properties of fluorine-18. However, extensive first-pass metabolism of [^{18}F]MDL100907 is expected to result in the formation of brain-penetrating radiometabolites [40], while *R*-[^{18}F]MH.MZ exhibits slow brain kinetics [38,39] and may be subject to active export by P-gp [41]. Alternatively, SPECT imaging with 5-[^{123}I]iodo-R91150 ([^{123}I]R93274), a radioiodinated analog of the potent and selective 5-HT_{2A} receptor antagonist R91150 (Fig. 1B), has been extensively used in preclinical and clinical studies [42–49]. While the widespread availability of SPECT facilities makes [^{123}I]R93274 an attractive tool for investigation of 5-HT_{2A} receptors in the brain, its applicability for quantitative studies is restricted by the lower spatial resolution and limited quantifiability of SPECT compared to PET. In addition, radioiodination increases the lipophilicity of [^{123}I]R93274 compared to the parent compound R91150 more than 10-fold [50], which leads to higher non-specific binding and thereby reduces the attainable signal-to-noise ratios. With this in mind, the PET tracer candidate [^{18}F]R91150 (Fig. 1B) with the more desirable physicochemical properties of the parent compound R91150 was prepared [50,51]. Initial *ex vivo* biodistribution studies in mice revealed good brain uptake of [^{18}F]R91150 and no formation of brain-derived radiometabolites for at least 30 min [50]. In addition, *in vitro* autoradiography in rat brain slices demonstrated a distribution pattern consistent with selective binding to 5-HT_{2A} receptors and a low degree of non-specific binding [51]. However, a more detailed evaluation of [^{18}F]R91150 by *in vivo* PET imaging is still lacking, as existing production methods afforded the probe in amounts insufficient for extensive preclinical evaluations. Thus, conventional protocols for the preparation of radiolabeled (hetero)aromatics using no-carrier-added (n.c.a.) [^{18}F]fluoride are mostly restricted to electron-deficient substrates, so that the preparation of radiofluorinated arenes labeled at non-activated or electron-rich positions (such as the fourth position of the phenoxy ring in [^{18}F]R91150) by these methods often requires complicated multistep approaches. Accordingly, the original radiosynthesis of [^{18}F]R91150 via S_NAr radiofluorination consisted of six reaction steps and afforded the tracer in non-decay-corrected radiochemical yields (activity yields, AYs) of only 0.5–1.7% after more than 190 min of synthesis time [50]. In contrast, Cu-mediated radiofluorination of (aryl)(mesityl)iodonium salts [52], aryl boronates [53,54] or trialkyl stannanes [55] enables the direct preparation of ^{18}F-labeled (hetero)aromatics using n.c.a. [^{18}F]fluoride regardless of their electronic properties. As such, application of alcohol-enhanced Cu-mediated radiofluorination of the corresponding *N*-Boc-protected pinacol boronate precursor afforded [^{18}F]R91150 in improved yields and enabled a first *in vitro* evaluation of the probe [51]. However, there was still a need for more efficient preparation procedures for *in vivo* applications. In the present article, we describe improved protocols for the production of [^{18}F]R91150 using a *NextGen* Cu-mediator [56], as well as the corresponding reference compound and radiofluorination precursors. In addition, we performed a preclinical evaluation of [^{18}F]R91150 by μPET imaging in mice and rats to assess its *in vivo* biodistribution, stability and binding behavior.

2. Results and discussion

2.1. Preparation of radiolabeling precursors and reference compound

According to our previous observations [57], aromatic amino groups are compatible with the protocol for alcohol-enhanced Cu-mediated radiofluorination, making it suitable for one-step preparation of ^{18}F-labeled anilines like [^{18}F]R91150 from appropriate non-protected precursors. In order to evaluate the efficacy of such a one-step procedure, we prepared the non-protected radiolabeling precursor **1** and the

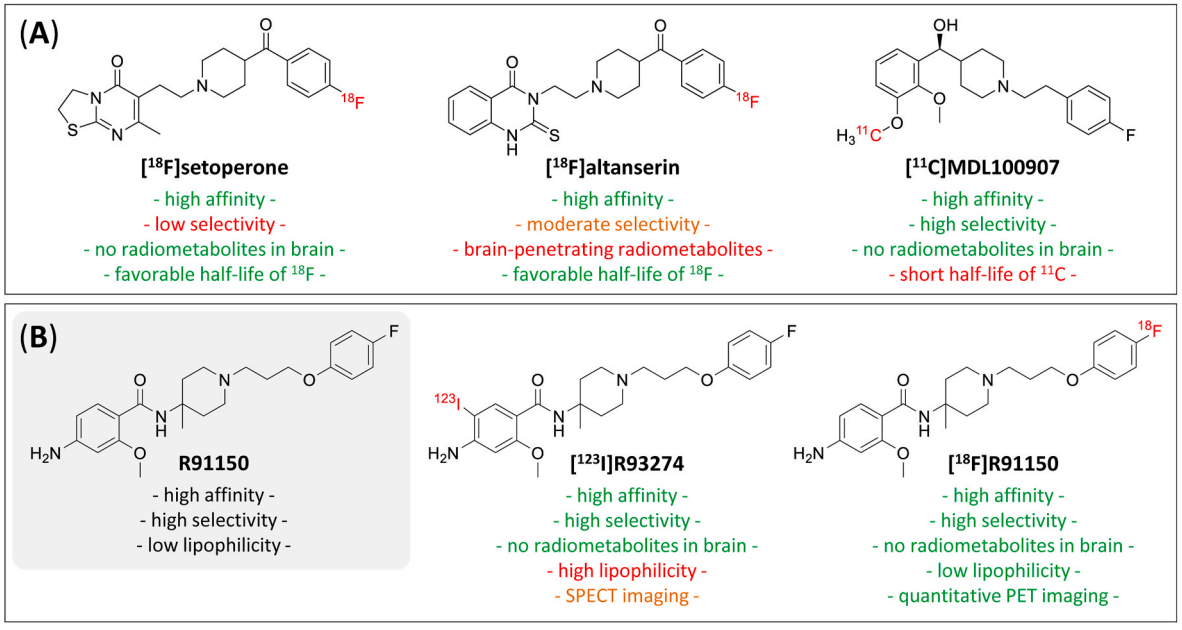

Fig. 1. Brief summary of radiolabeled 5-HT_{2A} receptor antagonists used as imaging agents. (**A**) Established PET radioligands. (**B**) R91150 and derived radioligands for SPECT ([^{123}I]R93274) or PET ([^{18}F]R91150) imaging.

reference compound R91150 as follows (Scheme 1). First, the substituted phenoxypropyl bromides **3a** [58] and **3b** [59] were conveniently prepared by alkylation of the respective phenols (**2a** and **2b**) with an eight-fold excess of 1,3-dibromopropane, which afforded the desired intermediates in yields of 75% and 55%, respectively.

For preparation of the reference compound R91150, commercially available *tert*-butyl 4-amino-4-methylpiperidine-1-carbamate (**4**) was then alkylated with **3a** to afford intermediate **5**, which was Boc deprotected and acylated with 2-methoxy-4-nitrobenzoyl chloride (prepared *in situ* from the respective acid). Finally, the NO_2-substituted intermediate **6a** thus obtained was reduced with Zn/NH_4Cl in EtOAc/EtOH according to Renk et al. [60] to obtain R91150 in 17% total yield over four steps. For preparation of the non-protected radiolabeling precursor, the amino amide **9** was synthesized from *tert*-butyl 4-amino-4-methylpiperidine-1-carboxylate (**7**) and 2-methoxy-4-nitrobenzoic acid in 49% yield over two steps. Subsequent alkylation of **9** with **3b** furnished the NO_2-substituted intermediate **6b**, which was reduced with Zn/NH_4Cl in EtOAc/EtOH to obtain the radiolabeling precursor **1** in 70% yield over two steps.

Due to the limited shelf life of precursor **1** under ambient conditions (see below), we also prepared the corresponding *N*-Boc protected radiolabeling precursor **10.** Since direct *N*-Boc protection of **1** proved to be inefficient under all reaction conditions examined, the synthesis of **10** was instead performed by an alternative protocol that started with Cbz-protection of **4** followed by removal of the Boc-group to obtain the mono-protected diamine **11** in 75% yield over two steps (Scheme 2).

11 was then acylated with *N*-Boc protected 4-amino-2-methoxybenzoic acid **12** [50] using azabenzotriazole tetramethyluronium hexafluorophosphate (HATU) as coupling agent to furnish intermediate **14** in 49% yield. Alternatively, conversion of **12** into the bench stable 2,3,5,6-tetrafluorophenyl active ester **13** followed by acylation of **11** with **13** gave **14** in 62% yield over two steps. Subsequent Cbz-deprotection by catalytic hydrogenation over Pd/C followed by alkylation of the resulting intermediate with **3b** afforded the desired radiolabeling precursor **10** in 24% or 30% total yield over five or six steps, respectively. Thus, compared to existing methods for preparation of R91150 and radiolabeling precursor **10,** which are rather laborious and low-yielding (3−7% over 6−7 steps [51]), the developed protocols afforded the desired compounds in > 2-fold (R91150) and > 8-fold (**10**) higher yields, respectively.

2.2. Radiosynthesis of [^{18}F]R91150

To prepare [^{18}F]R91150, we first optimized the conditions for Cu-mediated radiofluorination of the unprotected radiolabeling precursor **1** (for details see section 2.1 in the supporting information). The best results were obtained when the radiosynthesis was performed as follows (Scheme 3). [^{18}F]Fluoride ([^{18}F]F^-) was loaded onto an anion exchange resin and eluted with a solution Et_4NOTf (4 μmol) in MeOH. The solvent was removed under reduced pressure in a stream of argon and a solution

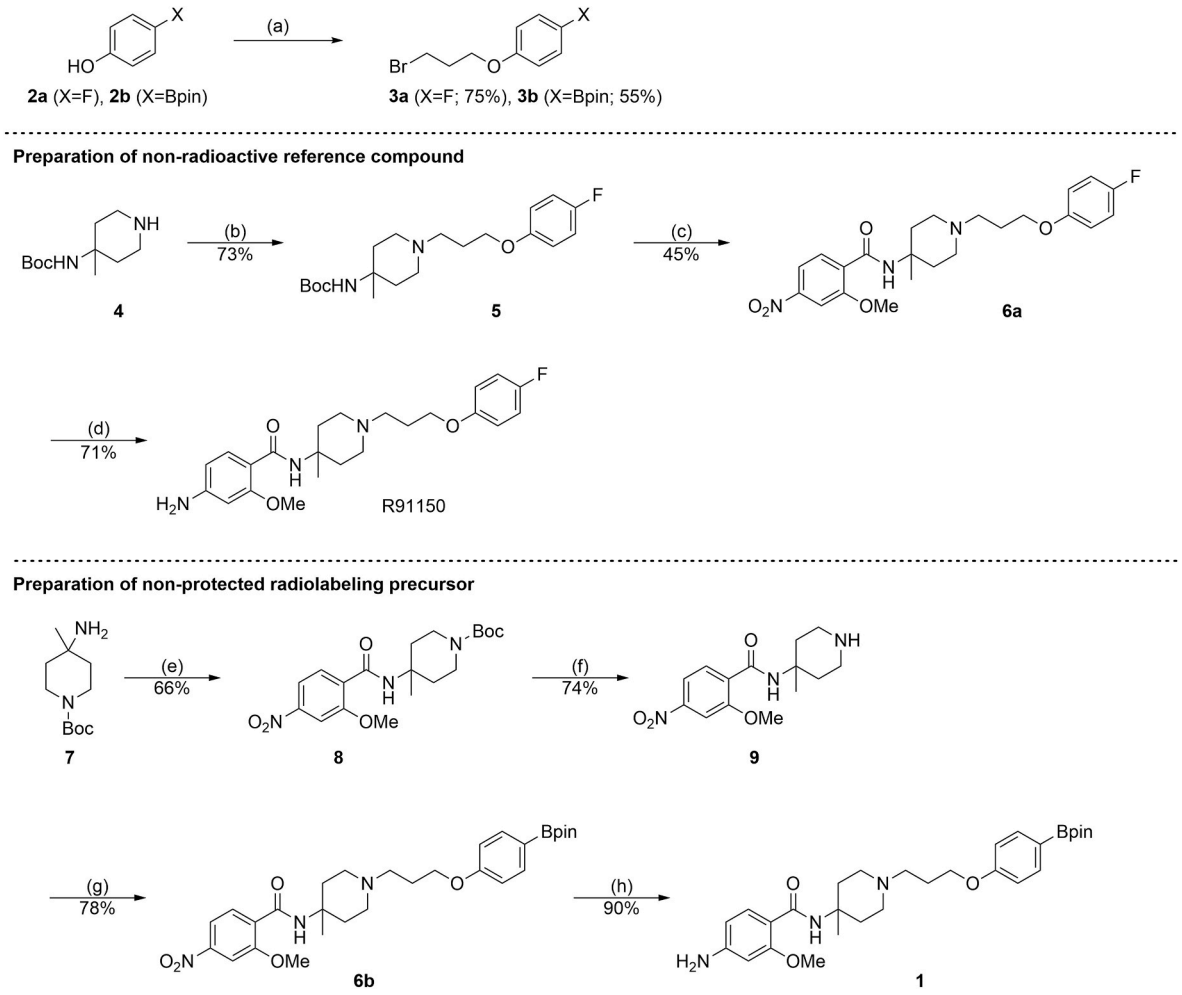

Scheme 1. Preparation of R91150 and non-protected radiolabeling precursor **1**. Conditions: (a) 1,3-dibromopropane, K_2CO_3, MeCN, 70 °C, 7 h; (b) **3a**, K_2CO_3, KI, DMF, rt, 16 h; (c) i. TFA/TIS/H_2O (95:2.5:2.5 v/v), ii. sat. $NaHCO_3$, iii. 2-methoxy-4-nitrobenzoyl chloride, DIPEA, CH_2Cl_2, rt, 1 h; (d) Zn/NH_4Cl, EtOH/EtOAc, rt, 3 h; e) 2-methoxy-4-nitrobenzoyl chloride, DIPEA, CH_2Cl_2, rt, 1 h; (f) i. TFA/TIS/H_2O (95:2.5:2.5 v/v), ii. sat. $NaHCO_3$; (g) **3b**, K_2CO_3, KI, DMF, rt, 16 h; (h) Zn/NH_4Cl, EtOH/EtOAc, rt, 12 h. Abbreviations: DIPEA – *N*,*N*-diisopropylethylamine, DMF – *N*,*N*-dimethylformamide, TFA – trifluoroacetic acid, TIS – triisopropylsilane.

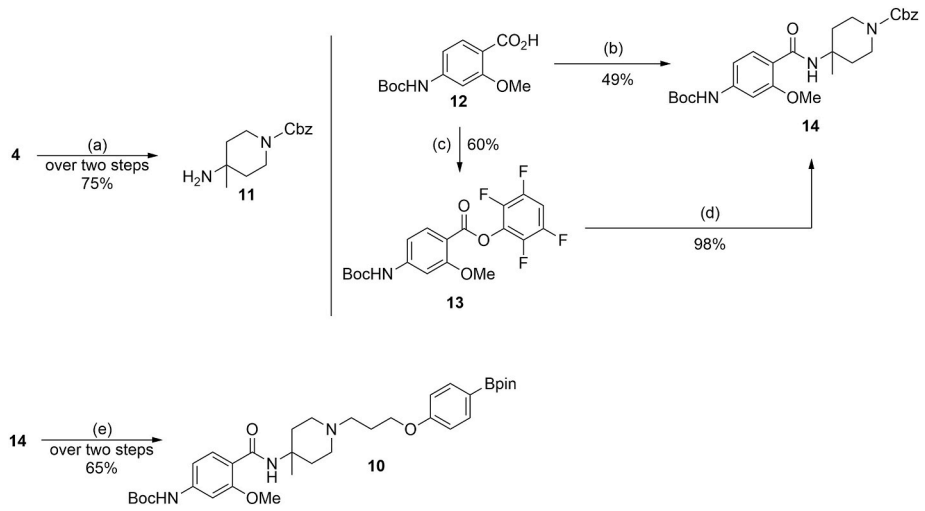

Scheme 2. Synthesis of *N*-Boc protected radiolabeling precursor **10**. Conditions: (a) i. Cbz-Cl, K_2CO_3, THF, rt, 1.5 h, ii. 20% TFA in CH_2Cl_2, rt, 16 h, iii. sat. $NaHCO_3$; (b) **11**, HATU, DIPEA, DMF, rt, 4 h; (c) 2,3,5,6-tetrafluorophenol, EDC, CH_2Cl_2, rt, 26 h; (d) **11**, DIPEA, DMF, 60 °C, 16 h; (e) i. Pd/C, H_2, MeOH, rt, 16 h, ii. **3b**, K_2CO_3, KI, DMF, rt, 4 h. Abbreviations: Cbz-Cl – benzyl chloroformate; DIPEA – *N*,*N*-diisopropylethylamine, DMF – *N*,*N*-dimethylformamide, EDC – 1-ethyl-3-(3-dimethylaminopropyl)carbodiimide hydrochloride, HATU – azabenzotriazole tetramethyluronium hexafluorophosphate, TFA – trifluoroacetic acid, THF – tetrahydrofuran.

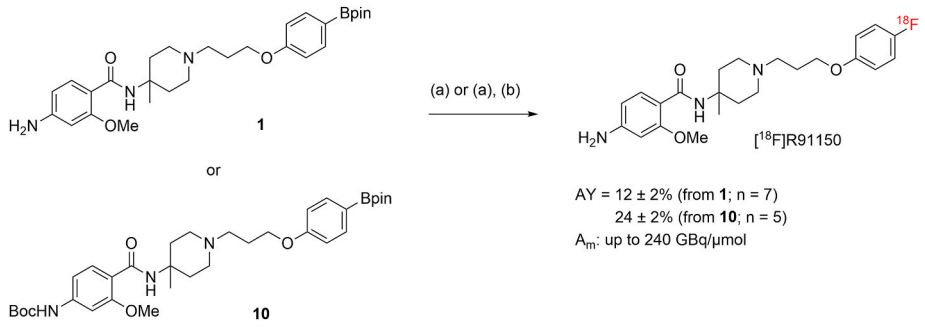

Scheme 3. Preparation of [^{18}F]R91150 from non-protected precursor **1** or *N*-Boc-protected precursor **10**. Conditions: (a) [^{18}F]F^- elution with Et_4NOTf (1 mg, 4 μmol) in MeOH (500 μL) followed by removal of MeOH and addition of **1** (5 μmol) or **10** (10 μmol) and $Cu(4\text{-}PhPy)_4(ClO_4)_2$ (10 μmol) in DMI/*n*BuOH (2:1), then 110 °C, 10 min, under air. (b) for preparation from **10**: 6 M HCl, 80 °C, 10 min. Abbreviations: [^{18}F]F^- – [^{18}F]fluoride, AY – activity yield, A_m – molar activity.

of precursor **1** (5 μmol) and $Cu(4\text{-}PhPy)_4(ClO_4)_2$ (10 μmol) in 1,3-dimethyl-2-imidazolidinone (DMI)/*n*BuOH (2:1) was added. The reaction mixture was then heated at 110 °C for 10 min under air to afford the crude radiotracer in radiochemical conversions (RCCs) of 35–46% (n = 5). The bulk of the high-boiling DMI/*n*BuOH was removed by solid phase extraction (SPE) to obtain a crude product solution suitable for HPLC purification. After HPLC purification and formulation, [^{18}F]R91150 was obtained as a ready-to-use solution in activity yields (AYs) of 12 ± 2% (n = 7) within 65–75 min. The molar activity (A_m) of the radiotracer after formulation amounted to 240 GBq/μmol for 1.03 GBq tracer. Quality control of the formulated tracer by HPLC demonstrated the absence of radiolabeled impurities. However, determination of the radiochemical purity (RCP) was complicated by significant retention of radioactivity on the applied C18 columns. Based on additional HPLC and TLC analyses (for details see section 3 in the supporting information), the latter was attributed to adsorption of intact [^{18}F]R91150 on RP stationary phases and the RCP of the formulated tracer was estimated to be ≥ 93%. Taken together, this protocol enabled one-step preparation of [^{18}F]R91150 in AYs comparable to those previously obtained using a two-step procedure [51], making it more suitable for automation. However, handling and storage of the unprotected radiolabeling precursor **1** was complicated by its hygroscopicity and limited shelf life under ambient conditions. To avoid these obstacles, we employed the same conditions for radiofluorination of the *N*-Boc-protected Bpin ester **10** (10 μmol) as a more stable radiolabeling precursor (Scheme 3), which afforded the ^{18}F-labeled intermediate Boc-[^{18}F]R91150 in RCCs of 70–86% (n = 6). Following removal of the reaction solvents by SPE as described above, the intermediate was deprotected with 6 M HCl at 80 °C for 10 min. Finally, HPLC purification and formulation furnished [^{18}F]R91150 as a ready-to-use solution in AYs of 24 ± 2% (n = 5) within 90–100 min and with an A_m of up to 217 GBq/μmol (1.46 GBq tracer) after formulation. Thus, compared to the original protocol described by Willmann et al. [51], application of the *NextGen* $Cu(4\text{-}PhPy)_4(ClO_4)_2$ in DMI/*n*BuOH [56] instead of the conventional $Cu(Py)_4(OTf)_2$ in DMA/*n*BuOH significantly improved the AYs of the two-step radiosynthesis by more than two-fold (24% vs. 10%).

2.3. Preclinical in vivo evaluation of [^{18}F]R91150

Having established an efficient protocol for the preparation of [^{18}F]R91150, we next evaluated the *in vivo* properties of the tracer by biodistribution studies in rodents. The whole body distribution and excretion of [^{18}F]R91150 were studied by μPET measurements in healthy mice (n = 4), which revealed a low background uptake into muscles and other 5-HT_{2A}-negative tissues (Fig. 2A). In addition, low accumulation of radioactivity in bones indicated sufficient stability of the probe against *in vivo* defluorination (Fig. 2). Excretion of [^{18}F]R91150 in mice was mainly hepatobiliary, with high tracer accumulation in gall bladder

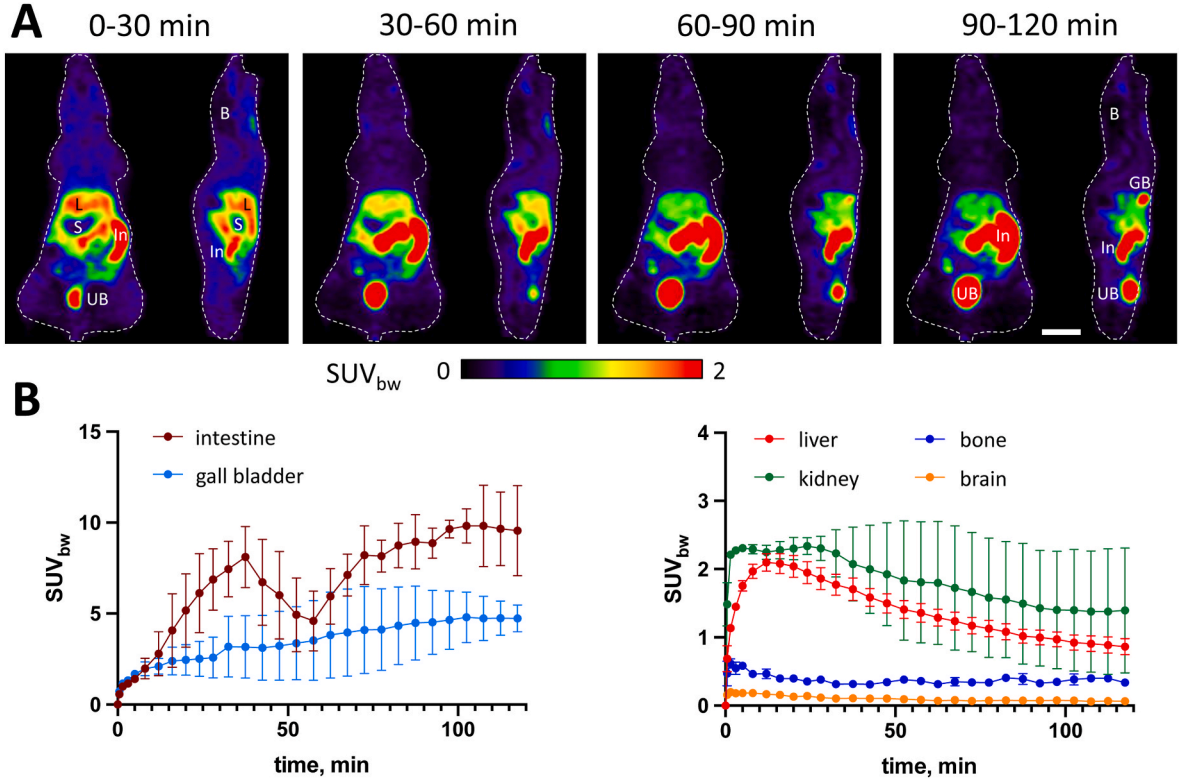

Fig. 2. *In vivo* biodistribution of [^{18}F]R91150 in healthy mice. (A) Representative horizontal (left) and sagittal (right) summed μPET images for the indicated time periods after tracer injection. White outlines indicate body contours. (B) Time-activity curves (mean ± standard deviation, n = 4) for volumes of interest placed in the indicated organs or tissues. Scale bar: 10 mm. Abbreviations: B - brain, GB - gall bladder, In - intestines, L - liver, S - stomach, UB - urinary bladder.

and intestines (Fig. 2). Apart from the presence of radiometabolites in feces, high radioactivity uptake in the intestines could in part reflect tracer binding to 5-HT$_{2A}$ receptors present in the enteric nervous system of both small intestine and colon [61]. However, the travel of radioactive bowel contents during the 2 h measurements was clearly visible (Suppl. Fig. S23). In contrast, liver uptake due to hepatic metabolism and possibly binding to 5-HT$_{2A}$ receptors present in the liver [62] was relatively low (Fig. 2).

Next, brain uptake and the cerebral distribution of [^{18}F]R91150 were evaluated by μPET measurements in healthy rats (n = 3) as a preclinical species that allows for more reliable assessment of the exact brain distribution (Figs. 3 and 4). Brain uptake of the probe was rapid, with cortical radioactivity accumulation reaching its peak within the first 2 min after tracer injection (Suppl. Fig. S24) and remaining relatively stable throughout the remaining measurement period (Figs. 3 and 4). The distribution pattern in the brain of naïve rats (Fig. 3A and 4A, top rows) was similar to that previously observed in *in vitro* autoradiography experiments with [^{18}F]R91150 [51]. In particular, radioactivity uptake was pronounced in the cortex and subcortical forebrain structures but low in the cerebellum and midbrain, which is consistent with the expression pattern of 5-HT$_{2A}$ receptors demonstrated by immunohistochemistry [63] and *in situ* hybridization [64,65]. In addition, pretreatment with 1.5 mg/kg altanserin (Fig. 3A, middle row) or displacement with 1.5 mg/kg ketanserin at 60 min after tracer injection (Fig. 3A, bottom row) reduced tracer uptake in the cerebral cortex by approximately 25–50% (Fig. 3B–top row), indicating selective and reversible binding of [^{18}F]R91150 to cortical 5-HT$_{2A}$ receptors. For statistical analysis, standardized uptake values normalized by body weight (SUV$_{bw}$) were calculated for four consecutive 30 min time periods after tracer injection (Fig. 3B, bottom row), which revealed a significant main effect of the factor blocker ($p = 0.0268$) on tracer uptake in the somatosensory cortex. In addition, post-hoc testing demonstrated a significant ($p < 0.05$) reduction of cortical tracer uptake by altanserin pretreatment during all four time-periods and by ketanserin displacement at 90–120 min after tracer injection (i.e. 30–90 min after ketanserin administration) (Fig. 3B, bottom row). Similar results were observed in homologous blocking studies performed after pre-treatment with 1 mg/kg non-labeled R91150 (Fig. 4A, bottom row), which significantly reduced cortical tracer uptake at 0−30 and 30−60 min after tracer injection by 25–50% (Fig. 4B, bottom row). Taken together, these findings are in line with the reduction of cortical [^{18}F]R91150 binding to rat brain slices by 50–70% previously observed in *in vitro* autoradiography experiments with R91150, altanserin and other 5-HT$_{2A}$ receptor antagonist [51]. The somewhat more effective reduction observed in brain slices could potentially be explained by the relatively high blocker concentrations (1−2 μM [51]) used *in vitro* and/or by displacement of [^{18}F]R91150 from peripheral 5-HT$_{2A}$ receptors in the *in vivo* blocking studies. Moreover, while radioactivity accumulation in the skull was not associated with significant spillover into the somatosensory cortex at visual analysis (Fig. 3A and 4A), some contribution of bone uptake to the cortical signals in our study can not be excluded. Thus, while bone accumulation of radioactivity at baseline was low, it did exceed brain uptake and showed a very modest but significant increase over time (Fig. 3B and 4B, bottom rows). The latter could point to some degree of *in vivo* radiodefluorination of the tracer with subsequent bone deposition of [^{18}F]fluoride. However, the minor increase of bone uptake over time indicates that there was no pronounced defluorination of the tracer in rats, which is consistent with a previous radiometabolite study in mice that reported no formation of [^{18}F]fluoride for up to 30 min [50]. Interestingly, altanserin pretreatment and ketanserin displacement both significantly reduced skull uptake of radioactivity (Fig. 3B, bottom row), suggesting that part of the bone uptake may have been related to extracerebral binding of the tracer to 5-HT$_{2A}$ receptors, which are expressed in osteoblastic cells [66–69]. On the other hand, there was no significant effect of homologous blocking with non-labeled R91150 (Fig. 4B, bottom row), indicating that most of the bone uptake

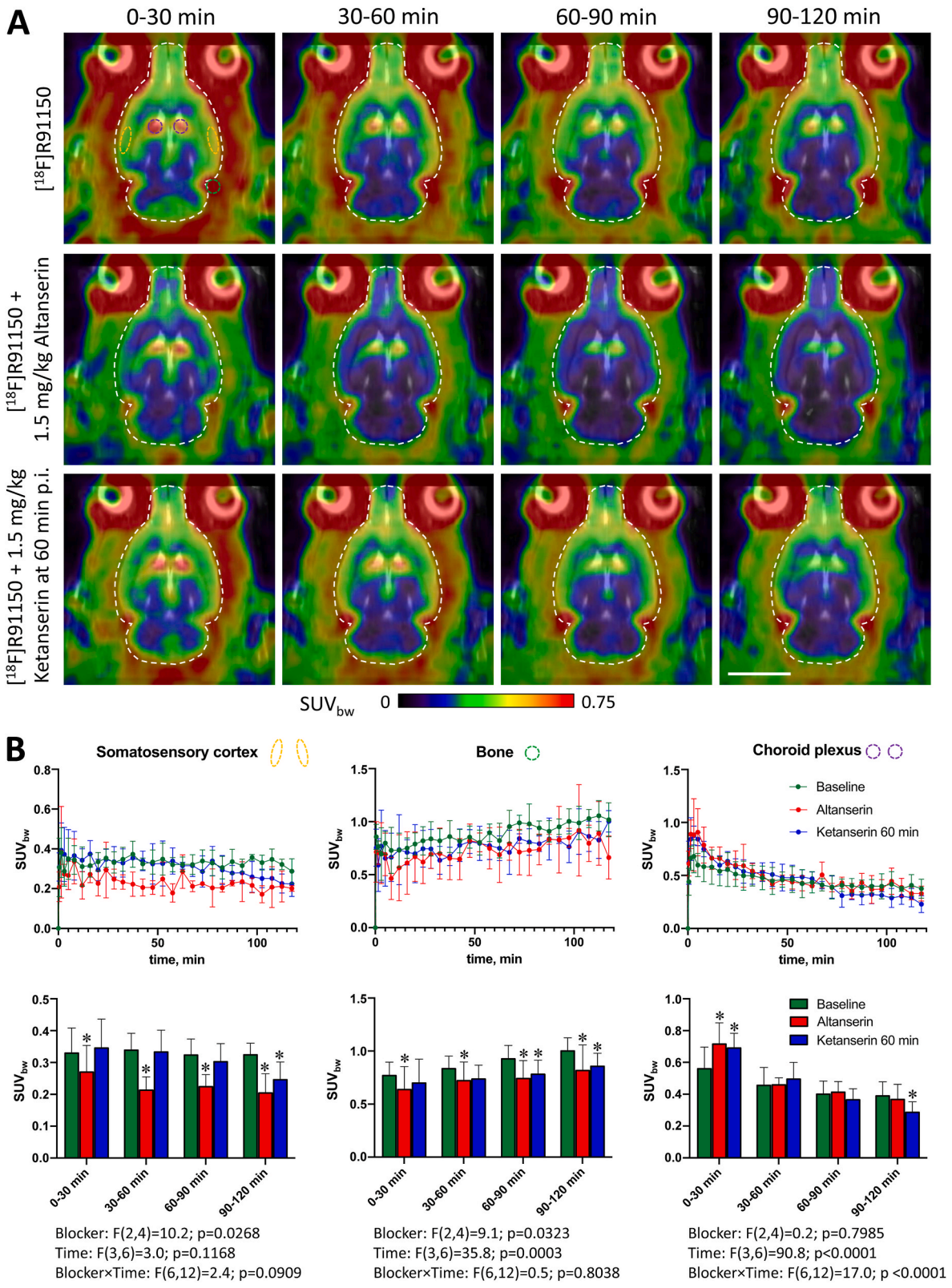

Fig. 3. *In vivo* brain distribution of [^{18}F]R91150 in healthy rats. (A) Representative summed PET images for the indicated time periods obtained in experiments with [^{18}F]R91150 alone (top row), after pretreatment with 1.5 mg/kg altanserin administered by intraperitoneal (i.p.) injection 50 min before tracer injection (middle row) and in displacement studies with 1.5 mg/kg ketanserin administered by intravenous (i.v.) injection 60 min after tracer injection (bottom row). PET images are projected onto an MRI template and the brain contours are indicated by white outlines. Scale bar: 10 mm. (B) Top row: Time-activity curves (mean ± standard deviation, n = 3) for volumes of interest (VOIs) placed in the somatosensory cortex, skull bone and choroid plexus. VOIs are indicated as dashed outlines in the [^{18}F]R91150/0–30 min image in A. Bottom row: Statistical analysis of the indicated time frames using a two-way repeated measures ANOVA followed by Dunnett's multiple comparison test. Main effects are indicated for each VOI. * indicates significant differences ($p < 0.05$) relative to baseline.

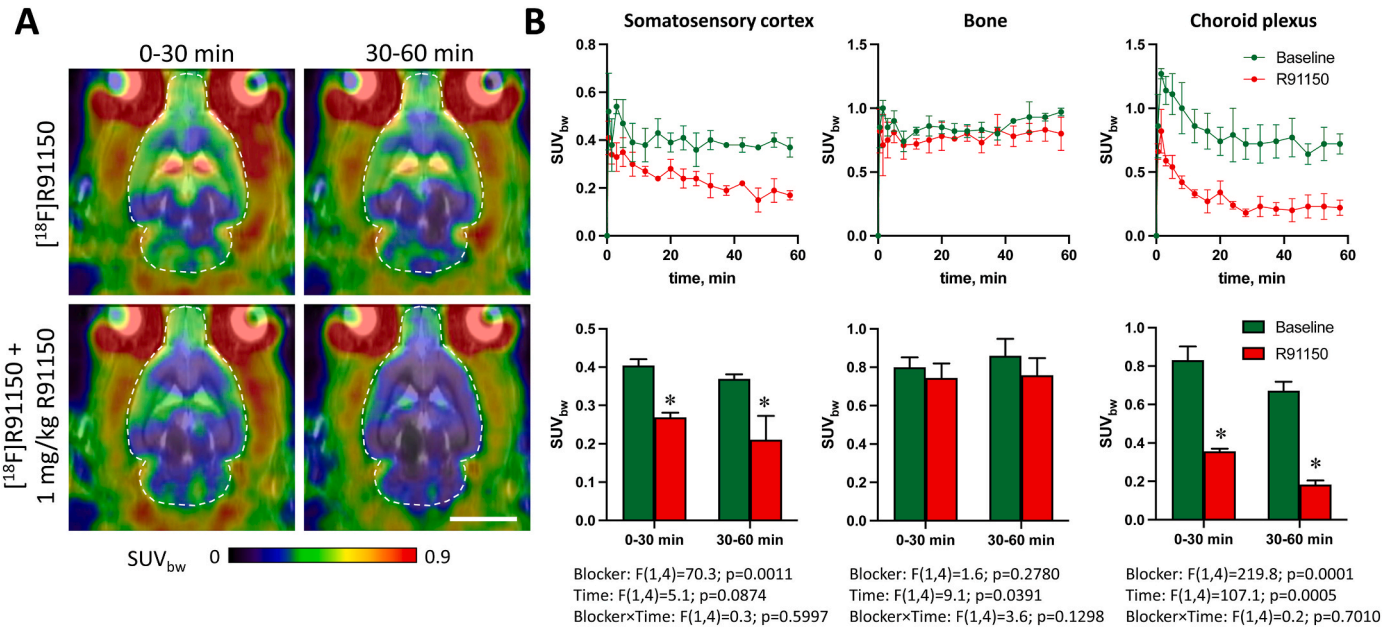

Fig. 4. Homologous blocking studies with non-labeled R91150 in healthy rats. (A) Representative summed PET images for the indicated time periods obtained in experiments with [^{18}F]R91150 alone (top row) and after pretreatment with 1 mg/kg R91150 administered by intravenous (i.v.) injection 5 min before tracer injection (bottom row). PET images are projected onto an MRI template and the brain contours are indicated by white outlines. Scale bar: 10 mm. (B) Top row: Time-activity curves (mean ± standard deviation, n = 3) for volumes of interest (VOIs) placed in the somatosensory cortex, skull bone and choroid plexus. For details on the exact placement of VOIs, see Fig. 3. Bottom row: Statistical analysis of the indicated time frames using a two-way repeated measures ANOVA followed by Sidak's multiple comparison test. Main effects are indicated for each VOI. * indicates significant differences ($p < 0.05$) relative to baseline.

was attributable to non-specific binding. Accordingly, further studies will be required to firmly establish and separate the mechanisms contributing to bone uptake of radioactivity as well as their effects on the quantification of 5-HT$_{2A}$ receptors in nearby brain regions.

Finally, considerable tracer uptake that was not reduced by pretreatment with altanserin and much less sensitive to displacement with ketanserin was also observed in the choroid plexus (Fig. 3), a region characterized by very high levels of 5-HT$_{2C}$ receptors [70]. Thus, as illustrated in Fig. 3B (bottom row), altanserin pretreatment actually increased tracer uptake in this region during the first 0–30 min after tracer injection and had no effect at the later time-points examined, while ketanserin displacement produced a moderate but significant

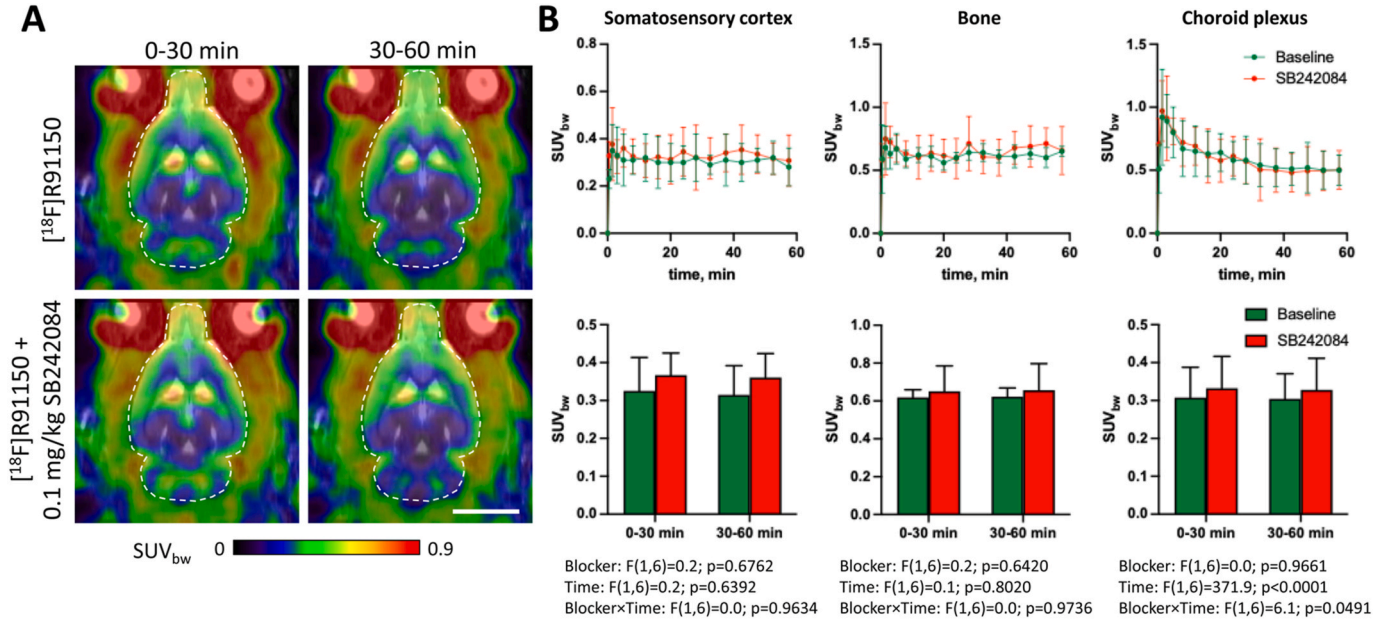

Fig. 5. Heterologous blocking studies with SB242084 in healthy rats. (A) Representative summed PET images for the indicated time periods obtained in experiments with [^{18}F]R91150 alone (top row) and after pretreatment with 0.1 mg/kg SB242084 administered by intraperitoneal (i.p.) injection 20 min before tracer injection (bottom row). PET images are projected onto an MRI template and the brain contours are indicated by white outlines. Scale bar: 10 mm. (B) Top row: Time-activity curves (mean ± standard deviation, n = 4) for volumes of interest (VOIs) placed in the somatosensory cortex, skull bone and choroid plexus. For details on the exact placement of VOIs, see Fig. 3. Bottom row: Statistical analysis of the indicated time frames using a two-way repeated measures ANOVA followed by Sidak's multiple comparison test. Main effects are indicated for each VOI.

decrease at 90–120 min. In contrast, homologous blocking with non-labeled R91150 resulted in a significant reduction of tracer uptake in the choroid plexus by approximately 50% at 0−30 min and 75% at 30−60 min after tracer injection (Fig. 4B), demonstrating that it was not related to non-specific binding. Although R91150 appears to be relatively selective (about 75-fold) for 5-HT_{2A} over 5-HT_{2C} receptors, it has been shown to inhibit binding of the 5-HT_{2C} ligand [^{3}H]mesulergine with an IC_{50} of 12.5 nM [71]. In addition, knockout of the 5-HT_{2C} receptor in mice completely abolished binding of [^{3}H]5-HT and several other 5-HT_2-targeting radioligands in the choroid plexus, suggesting very low or no expression of 5-HT_{2A} receptors in this region [72]. Accordingly, accumulation of [^{18}F]R91150 in the choroid plexus could at least in part represent binding to 5-HT_{2C} receptors, as has been reported for several other 5-HT_{2A} radioligands [65,73]. We therefore performed additional blocking studies with SB242084, a highly selective and brain penetrant 5-HT_{2C} receptor antagonist [74]. As illustrated in Fig. 5, pre-treatment with 0.1 mg/kg SB242084 had no significant effect on tracer accumulation in the choroid plexus or somatosensory cortex, suggesting that 5-HT_{2C} receptors do not contribute to [^{18}F]R91150 binding in these regions. Taken together, these findings indicate that [^{18}F]R91150 exhibits sufficient selectivity for 5-HT_{2A} over 5-HT_{2C} receptors, but may interact with some other membrane receptor expressed in the choroid plexus. However, given the particular abundance of transport proteins in the choroid plexus [75], accumulation of [^{18}F]R91150 in this region could also reflect a specific transporter-mediated process. For example, several radiolabeled substrates for efflux transporters expressed at the blood-cerebrospinal fluid (CSF) barrier have been shown to accumulate in the choroid plexus [76–78]. Accordingly, radioactivity uptake in this region could reflect active export of [^{18}F]R91150 from the CSF to the bloodstream. Subsequent clearance of the radiotracer via circulation could then account for the distinct kinetics of tracer accumulation in the choroid plexus, which was much less persistent than tracer accumulation in the cortex (Fig. 3−5). Alternatively, [^{18}F]R91150 could be subject to active transport into the ventricles followed by non-specific binding to ependymal and plexus tissue, a mechanism previously proposed to explain the ventricular accumulation of ^{18}F-labeled pyridinylphenyl amides [79]. In this case, lower radioactivity retention in the choroid plexus could be attributable to bulk flow of cerebrospinal fluid and/or diffusion of the tracer into surrounding brain tissue. Further studies on the specific binding or transport mechanism involved in ventricular uptake of [^{18}F]R91150 seem warranted, since our findings suggest that this radioligand could offer several unique advantages over other known 5-HT_{2A} receptor tracers. Thus, compared to 5-[^{123}I]iodo-R91150, [^{18}F]R91150 exhibits reduced non-specific binding and should enable quantitative PET imaging with improved signal-to-noise ratios. We also found no evidence for significant defluorination or the formation of brain-penetrating radiometabolites, which have been shown or are thought to complicate the application of existing radioligands like [^{18}F]altanserin [32] or [^{18}F]MDL100907 [40]. In addition, [^{18}F]R91150 showed rapid brain uptake, with cortical tracer uptake reaching steady-state within the first 2 min, in contrast to the slow brain kinetics of (*R*)-[^{18}F]MH.MZ, which reached steady-state after approximately 30 or 80 min in rats or humans, respectively [38,39]. This faster uptake of [^{18}F]R91150 could be advantageous, as it would allow for shorter scan times. Furthermore, [^{18}F]R91150 exhibited no evident binding to 5-HT_{2C} receptors, which complicates quantification of 5-HT_{2A} receptors in subcortical brain regions with dual 5-HT_{2A} and 5-HT_{2C} radioligands like [^{11}C]Cimbi-36 [73,80]. Finally, the favorable nuclear chracteristics of fluorine-18, including its longer half-life and lower positron energy, should enable broader clinical use of [^{18}F]R91150 compared to ^{11}C-labeled tracers like [^{11}C]MDL100907 or [^{11}C]Cimbi-36.

2.4. Conclusion

In conclusion, we have developed efficient protocols for the preparation of R91150 and two Bpin-substituted radiolabeling precursors for [^{18}F]R91150. Cu-mediated radiofluorination of the precursors afforded [^{18}F]R91150 in improved activity yields of 12–24% over one or two steps. This method addresses key limitations of previous radiosynthesis protocols, including low yields and complex multi-step processes, while providing a more streamlined and reliable approach. Preclinical evaluation of the probe by μPET imaging in rodents demonstrated that [^{18}F]R91150 could offer distinct advantages over other 5-HT_{2A} receptor radioligands, such as faster brain kinetics, reduced non-specific binding, and/or improved selectivity for 5-HT_{2A} over 5-HT_{2C} receptors. These features make [^{18}F]R91150 a promising candidate for PET imaging of 5-HT_{2A} receptors. However, further studies will be required to confirm sufficient radiotracer stability, firmly establish the exact mechanisms of skull uptake and tracer accumulation in the choroid plexus, and assess the ability of [^{18}F]R91150 PET imaging to detect (patho)physiological alterations of 5-HT_{2A} receptors in animal models.

3. Materials and methods

3.1. Chemistry

3.1.1. General conditions

Unless otherwise stated, all reagents and solvents were purchased from Sigma-Aldrich (Steinheim, Germany), Acros (Fisher Scientific GmbH, Nidderrau, Germany), Alfa Aesar [Thermo Fisher (Kandel) GmbH, Kandel, Germany], BLDPharm (Kaiserslautern, Germany) or Key Organics (Camelford, UK), and used without further purification. Unless otherwise stated, all reactions were carried out with magnetic stirring and, if air or moisture sensitive substrates and/or reagents were used, in flame-dried glassware under argon. Organic extracts were dried over anhydrous Na_2SO_4 or $MgSO_4$. Solutions were concentrated under reduced pressure (1–900 mbar) at 40–50 °C using a rotary evaporator. Column chromatography was performed with silica gel, 60 Å, 230–400 mesh particle size from VWR International GmbH (Darmstadt, Germany) or silica gel (w/Ca, 0.1%), 60 Å, 230–400 mesh particle size from Sigma-Aldrich GmbH (Steinheim, Germany). Thin layer chromatography (TLC) was performed using aluminum sheets coated with silica gel 0.25 mm SIL G/UV 254 (Merck KGaA, Darmstadt, Germany). Chromatograms were inspected under UV light (λ = 254 nm) and/or stained with phosphomolybdic acid (4 wt% in EtOH), ninhydrin (0.5 wt% in 1-butanol) or potassium permanganate solution (0.75 wt% $KMnO_4$, 5 wt% K_2CO_3 and 0.63 v% 10% NaOH in water). Proton, carbon and fluorine nuclear magnetic resonance (^{1}H-, ^{13}C and ^{19}F NMR) spectra were recorded on a Bruker Avance Neo (400 MHz) spectrometer. Chemical shifts are reported in parts per million (ppm) relative to residual peaks of deuterated solvents. The observed signal multiplicities are characterized as follows: s = singlet, d = doublet, t = triplet, p = pentet, m = multiplet, dd = doublet of doublets, dt = doublet of triplets, ddd = doublet of doublets of doublets and br = broad. Coupling constants (*J*) are reported in hertz (Hz). Electrospray ionization (ESI) low resolution mass spectra (LRMS) were measured with an MSQ PlusTM mass spectrometer (Thermo Electron Corporation, San Jose, USA). ESI high resolution mass spectra (HRMS) were measured with an LTQ Orbitrap XL (Thermo Fischer Scintific Inc., Bremen, Germany).

3.1.2. Organic syntheses

1-(3-Bromopropoxy)-4-fluorobenzene (3a) [81]**:** Anhydrous K_2CO_3 (19.6 g, 142 mmol, 1.6 eq.) was added to a solution of 1,3-dibromopropane (72.7 mL, 144 g, 713 mmol, 8 eq.) and 4-fluorophenol (**2a**) (10 g, 89.2 mmol, 1 eq.) in anhydrous MeCN (125 mL) and the resulting suspension was vigorously stirred at 70 °C for 16 h. The reaction mixture was allowed to cool to ambient temperature, filtered through Celite® and concentrated under reduced pressure. The crude product was purified by kugelrohr distillation at 10 mbar to afford the title compound (15.5 g, 66.5 mmol, 75%) as a colorless liquid. ^{1}H NMR (400 MHz,

$CDCl_3$): δ = 7.01–6.94 (m, 2H), 6.87–6.82 (m, 2H), 4.07 (t, *J* = 5.8 Hz, 2H), 3.60 (t, *J* = 6.4 Hz, 2H), 2.31 (dt, *J* = 5.8, 6.4 Hz, 2H). ^{13}C NMR (101 MHz, $CDCl_3$): δ = 157.51 (d, *J* = 239.4 Hz), 154.97 (d, *J* = 3.0 Hz), 115.91 (d, *J* = 23.2 Hz), 115.70 (d, *J* = 9.1 Hz), 66.11, 32.49, 30.07. ^{19}F NMR (376 MHz, $CDCl_3$): δ = −123.86. GC-HRMS (EI, 70 eV) *m/z*: $[M]^{\bullet+}$ calculated for $C_9H_{10}BrFO^+$: 233.98731, 231.98936; found: 233.9871, 231.9892.

2-[4-(3-Bromopropoxy)phenyl]-4,4,5,5-tetramethyl-1,3,2-dioxaborolane (3b) [59]**: 3b** (4.1 g, 12 mmol, 55%, colorless oil which solidified on standing) was prepared from 4-(4,4,5,5-tetramethyl-1,3,2-dioxaborolan-2-yl)phenol (4.8 g, 22 mmol, 1 eq.), 1,3-dibromopropane (18.0 mL, 35.7 g, 177 mmol, 8 eq.) and anhydrous K_2CO_3 (4.8 g, 35 mmol, 1.6 eq.) in anhydrous MeCN (125 mL) using the same procedure as described for **3a** and isolated by column chromatography (silica gel with 0.1% Ca, hexane/EOAc, 1.4:1). ^{1}H NMR (400 MHz, $CDCl_3$): δ = 7.75 (d, *J* = 8.7 Hz, 2H), 6.90 (d, *J* = 8.7 Hz, 2H), 4.13 (t, *J* = 5.8 Hz, 2H), 3.60 (t, *J* = 6.5 Hz, 2H), 2.32 (p, *J* = 6.2 Hz, 2H), 1.34 (s, 6H). ^{13}C NMR (101 MHz, $CDCl_3$) δ 161.37, 136.68, 113.98, 83.70, 65.22, 32.46, 30.06, 24.99. The signal of *C*-Bpin was not observed.

***tert*-Butyl {1-[3-(4-fluorophenoxy)propyl]-4-methylpiperidin-4-yl}carbamate (5):** Anhydrous K_2CO_3 (4.7 g, 34 mmol, 3.7 eq.) was added to a solution of **3a** (2.2 g, 9.5 mmol, 1.02 eq.), **4** (2.0 g, 9.3 mmol, 1 eq.), and KI (15 g, 93 mmol, 10 eq.) in anhydrous *N*,*N*-dimethylformamide (DMF, 10 mL) and the resulting suspension was vigorously stirred for 16 h. After filtration and concentration of the reaction mixture under reduced pressure, the residue was purified by column chromatography (hexane/EtOAc, 1.5:1) to afford the title compound (2.5 g, 6.8 mmol, 73%) as a colorless solid. ^{1}H NMR (400 MHz, $CDCl_3$): δ = 6.98–6.92 (m, 2H), 6.84–6.80 (m, 2H), 4.31 (s, 1H), 3.96 (t, *J* = 6.3 Hz, 2H), 2.66 (d, *J* = 11.5 Hz, 2H), 2.659–2.55 (m, 2H), 2.33 (t, *J* = 10.5 Hz, 2H), 2.03–1.96 (m, 4H), 1.67 (dt, *J* = 33.4, 11.5 Hz, 2H), 1.43 (s, 9H), 1.34 (s, 3H). ^{13}C NMR (101 MHz, $CDCl_3$): δ = 157.33 (d, *J* = 239.4 Hz), 155.18 (d, *J* = 1.0 Hz), 154.65, 115.88 (d, *J* = 22.2 Hz), 115.56 (d, *J* = 8.1 Hz), 79.11, 66.94, 55.30, 50.24, 49.57, 36.29, 28.59, 26.85, 26.49. The signal of *C*O-O*t*Bu was overlaid by one of the components of the *C*–F doublet (at 158.51 ppm). ^{19}F NMR (376 MHz, $CDCl_3$): δ = −124.17. LRMS (ESI) *m/z*: $[M+H]^+$ calculated for $C_{20}H_{32}FN_2N_2O_3^+$: 367.24; found: 367.29. HRMS (ESI) *m/z*: $[M+H]^+$ calculated for $C_{20}H_{32}FN_2N_2O_3^+$: 367.23915; found: 367.23895.

a) 1-[3-(4-Fluorophenoxy)propyl]-4-methylpiperidine-4-amine [50]

***N*-{1-[3-(4-Fluorophenoxy)propyl]-4-methylpiperidin-4-yl}-2-methoxy-4-nitrobenzamide (6a):**

A solution of **5** (2.45 g, 6.69 mmol, 1 eq.) in trifluoroacetic acid (TFA)/triisopropylsilane (TIS)/H_2O (20 mL, 95/2.5/2.5 v/v) was allowed to stand for 5 min at ambient temperature and concentrated under reduced pressure. The residue was taken up into toluene (50 mL) and the resulting emulsion was concentrated under reduced pressure (× 3). The residue was dissolved in EtOAc (100 mL) and the solution was washed with sat. $NaHCO_3$ (100 mL), dried and concentrated under reduced pressure to afford 1-[3-(4-fluorophenoxy)propyl]-4-methylpiperidine-4-amine (1.56 g, 5.86 mmol, 88%) as a colorless oil, which was used for the next step without further purification or characterization.

b) 2-Methoxy-4-nitrobenzoyl chloride [82]

DMF (one drop) was added to a suspension of 2-methoxy-4-nitrobenzoic acid (1.30 g, 6.59 mmol, 1.12 eq.) in oxalyl chloride (4.0 mL, 5.9 g, 46 mmol) and the resulting suspension was stirred until complete dissolution of the solids and cessation of gas evolution (approximately 15 min). The mixture was concentrated under reduced pressure, the residue was taken up into toluene (50 mL) and the resulting solution was concentrated under reduced pressure (× 3) to afford crude 2-methoxy-4-nitrobenzoyl chloride as a yellow oil, which was immediately used for the next step without further purification or characterization.

c) N-{1-[3-(4-Fluorophenoxy)propyl]-4-methylpiperidin-4-yl}-2-methoxy-4-nitrobenzamide (**6a**)

A solution of 2-methoxy-4-nitrobenzoyl chloride in anhydrous CH_2Cl_2 (10 mL) was added to a solution of 1-[3-(4-fluorophenoxy)propyl]-4-methylpiperidine-4-amine (1.56 g, 5.86 mmol, 1 eq.) and *N*,*N*-diisopropylethylamine (DIPEA, 2.0 mL, 1.5 g, 12 mmol, 2 eq.) in anhydrous CH_2Cl_2 (20 mL) and the resulting mixture was stirred for 1 h. The reaction mixture was then concentrated under reduced pressure and the residue was taken up into EtOAc and H_2O (80 mL of each). The organic layer was washed with 5% $NaHCO_3$ (3 × 40 mL), 1 M $NaHSO_4$ (3 × 40 mL), H_2O (3 × 40 mL) and brine (2 × 40 mL), and concentrated under reduced pressure. The residue was purified by column chromatography ($CHCl_3$/MeOH, 9:1) to afford **6a** (1.34 g, 3.01 mmol, 45% over three steps) as a faint yellow solid. ^{1}H NMR [400 MHz, $(CD_3)_2SO$]: δ = 7.88–7.85 (m, 2H), 7.78 (s, 1H), 7.74–7.71 (m, 1H), 7.13–7.06 (m, 2H), 6.95–6.90 (m, 2H), 3.99 (s, 3H), 3.96 (t, *J* = 6.8 Hz, 2H), 2.57 (d, *J* = 11.2 Hz, 2H), 2.42 (t, *J* = 6.8 Hz, 2H), 2.23 (t, *J* = 11.2 Hz, 2H), 2.17 (t, *J* = 16.4 Hz, 2H), 1.86 (p, *J* = 6.6 Hz, 2H), 1.50 (dd, *J* = 16.4, 6.6 Hz, 2H), 1.37 (s, 3H). ^{13}C NMR [101 MHz, $(CD_3)_2SO$]: δ = 163.47, 157.55, 156.83 (d, *J* = 236.3 Hz), 155.20, 154.98 (d, *J* = 2.0 Hz), 148.99, 131.96, 130.39, 115.78 (d, *J* = 20.2 Hz), 115.63 (d, *J* = 5.1 Hz), 115.45, 106.83, 66.43, 56.59, 54.62, 51.55, 49.03, 35.43, 26.40, 26.17. ^{19}F NMR [376 MHz, $(CD_3)_2SO$]: δ = −124.26. LRMS (ESI) *m/z*: $[M+H]^+$ calculated for $C_{23}H_{29}FN_3O_5^+$: 446.21; found: 446.26. HRMS (ESI) *m/z*: $[M+H]^+$ calculated for $C_{23}H_{29}FN_3O_5^+$: 446.20858; found: 446.20877.

4-Amino-*N*-{1-[3-(4-fluorophenoxy)propyl]-4-methylpiperidin-4-yl}-2-methoxybenzamide (R91150) [50]**:** NH_4Cl (0.4 g, 7 mmol) followed by Zn dust (0.5 g, 7 mmol, 10 eq.) were added to a solution of **6a** (0.3 g, 0.7 mmol, 1 eq.) in 50% EtOH in EtOAc (50 mL) and the resulting suspension was vigorously stirred for 3 h. The reaction mixture was then filtered through Celite® and concentrated under reduced pressure. The residue was purified by column chromatography ($CHCl_3$/MeOH, 9:1) to afford the title compound (0.2 g, 0.5 mmol, 71%) as a colorless foam. In some runs, the reaction did not go to completion and afforded a mixture of partially reduced intermediates (mainly the corresponding azoxyarene according to MS-spectra). In such cases, the reaction mixture was filtered through Celite®, concentrated under reduced pressure and the residue was taken up into 50% EtOH in EtOAc (125 mL/g). Zn and AcOH (10 eq. of each) were added and the reaction mixture was vigorously stirred for 16 h. The reaction mixture was then filtered through Celite®, concentrated under reduced pressure and the residual crude product was purified by column chromatography on silica ($CHCl_3$/MeOH, 9:1) followed by C_{18}-MPLC or -HPLC to afford R91150 in 30–40% yield as a yellow oil or foam. ^{1}H NMR (400 MHz, $CDCl_3$): δ = 7.96 (d, *J* = 8.5 Hz, 1H), 7.62 (s, 1H), 6.97–6.891 (m, 2H), 6.84–6.79 (m, 2H), 6.33 (dd, *J* = 8.5, 2.1 Hz, 1H), 6.20 (d, *J* = 2.1 Hz, 1H), 4.00 (s, 2H), 3.96 (t, *J* = 6.3 Hz, 2H), 3.89 (s, 3H), 2.73 (d, *J* = 11.8 Hz, 2H), 2.54 (dd, *J* = 16.4, 9.2 Hz, 2H), 2.30 (t, *J* = 11.8 Hz, 2H), 2.22 (t, *J* = 16.4 Hz, 2H), 2.01–1.95 (m, 2H), 1.74 (dt, *J* = 19.9, 4.5 Hz, 2H), 1.50 (s, 3H). ^{13}C NMR (101 MHz, $CDCl_3$): δ = 164.79, 158.96, 157.27 (d, *J* = 238.4 Hz), 155.24 (d, *J* = 2.0 Hz), 150.87, 133.71, 115.97, 115.74 (d, *J* = 23.2 Hz), 115.51 (d, *J* = 8.1 Hz), 112.98, 107.84, 97.43, 67.01, 55.88, 55.45, 51.22, 49.74, 36.51, 26.94, 26.66. ^{19}F NMR (376 MHz, $CDCl_3$): δ = −124.23. LRMS (ESI) *m/z*: $[M+H]^+$ calculated for $C_{23}H_{31}FN_3O_3^+$: 416.23; found: 416.29. HRMS (ESI) *m/z*: $[M+H]^+$ calculated for $C_{23}H_{31}FN_3O_3^+$: 416.23440; found: 416.23454.

***tert*-Butyl 4-(2-methoxy-4-nitrobenzamido)-4-methylpiperidine-1-carboxylate (8):** A solution of 2-methoxy-4-nitrobenzoyl chloride [prepared from 2-methoxy-4-nitrobenzoic acid (2.0 g, 9.9 mmol, 1.06 eq.) and oxalyl chloride (5.0 mL, 7.4 g, 58 mmol) as described above for the synthesis of **6a**] in anhydrous CH_2Cl_2 (10 mL) was added to a solution of *tert*-butyl 4-amino-4-methylpiperidine-1-carboxylate (**7**) (2.0 g, 9.3 mmol, 1 eq.) and DIPEA (3.4 mL, 2.5 g, 19 mmol, 2 eq.) in anhydrous CH_2Cl_2 (50 mL) and the resulting mixture was stirred for 1 h. The reaction mixture was then concentrated under reduced pressure and the residue was taken up into EtOAc and H_2O (80 mL of each). The organic layer was washed with 5% $NaHCO_3$ (3 × 40 mL), 1 M $NaHSO_4$ (3 × 40 mL), H_2O (3 × 40 mL) and brine (2 × 40 mL), and concentrated under reduced pressure. The residue was purified by

column chromatography (hexane/$CHCl_3$/EtOAc/MeOH, 20:9:8:1) to afford the title compound (2.4 g, 6.1 mmol, 66%) as a faint yellow solid. ^{1}H NMR [400 MHz, $(CD_3)_2CO$]: δ = 8.06 (dd, *J* = 8.4, 0.3 Hz, 1H), 7.92 (d, *J* = 2.0 Hz, 1H), 7.90–7.85 (m, 1H), 7.70 (s, 1H), 4.15 (s, 3H), 3.79 (d, *J* = 13.7 Hz, 2H), 3.24–3.06 (m, 2H), 2.34–2.18 (m, 2H), 1.58–1.50 (m, 2H), 1.49 (s, 3H), 1.44 (s, 9H). ^{13}C NMR [101 MHz, $(CD_3)_2CO$]: δ = 163.79, 158.46, 155.12, 150.89, 132.65, 130.90, 116.28, 107.77, 79.42, 57.40, 52.98, 36.44, 28.58, 26.45. LRMS (ESI) *m/z*: $[M+H]^+$ calculated for $C_{19}H_{28}N_3O_6^+$: 394.20; found: 394.22. HRMS (ESI) *m/z*: $[M+Na]^+$ calculated for $C_{19}H_{27}N_3O_6Na^+$: 416.17921; found: 416.17991.

2-Methoxy-*N*-(4-methylpiperidin-4-yl)-4-nitrobenzamide (9): A solution of **8** (2.35 g, 5.97 mmol, 1 eq.) in TFA/TIS/H_2O (95:2.5:2.5, 10 mL) was allowed to stand for 5 min at ambient temperature and then concentrated under reduced pressure. The residue was taken up into toluene (50 mL) and the resulting emulsion was concentrated under reduced pressure (× 3). The residue was dissolved in EtOAc (100 mL) and the solution was washed with sat. $NaHCO_3$ (100 mL), dried and concentrated under reduced pressure to afford the title compound (1.3 g, 4.4 mmol, 74%) as a yellow solid. ^{1}H NMR [400 MHz, $(CD_3)_2CO$]: δ = 7.95–7.87 (m, 3H), 7.76 (s, 1H), 4.14 (s, 3H), 3.45–3.33 (m, 4H), 2.60 (d, *J* = 13.1 Hz, 2H), 1.99 (ddd, *J* = 12.2, 7.4, 5.2 Hz, 2H), 1.54 (s, 3H). ^{13}C NMR [101 MHz, $(CD_3)_2CO$]: δ = 164.80, 158.34, 150.85, 132.11, 131.69, 116.30, 107.61, 57.29, 51.75, 40.85, 33.20, 26.62. LRMS (ESI) *m/z*: $[M+H]^+$ calculated for $C_{14}H_{20}N_3O_4^+$: 294.15; found: 294.11. HRMS (ESI) *m/z*: $[M+H]^+$ calculated for $C_{14}H_{20}N_3O_4^+$: 294.14483; found: 294.14510.

2-Methoxy-*N*-(4-methyl-1-{3-[4-(4,4,5,5-tetramethyl-1,3,2-dioxaborolan-2-yl)phenoxy]-propyl}piperidin-4-yl)-4-nitrobenzamide (6b): 6b (3.1 g, 5.6 mmol, 78%, faint yellow solid) was prepared from **9** (2.1 g, 7.2 mmol, 1 eq.), **3b** (2.5 g, 7.3 mmol, 1.01 eq.), anhydrous K_2CO_3 (1.0 g, 7.2 mmol, 1 eq.) and KI (1.2 g, 7.23 mmol) in anhydrous DMF (25 mL) using the same procedure as described for **6a**. The crude product was purified by column chromatography (silica gel with 0.1% Ca, $CHCl_3$/MeOH, 11:1). ^{1}H NMR (400 MHz, $CDCl_3$): δ = 8.28 (d, *J* = 8.6 Hz, 1H), 7.92 (dd, *J* = 8.6, 2.1 Hz, 1H), 7.84 (d, *J* = 2.0 Hz, 1H), 7.72 (t, *J* = 5.4 Hz, 2H), 7.55 (s, 1H), 6.86 (d, *J* = 8.6 Hz, 2H), 4.08 (s, 3H), 4.04 (t, *J* = 6.1 Hz, 2H), 2.92–2.80 (m, 2H), 2.68 (t, *J* = 7.1 Hz, 2H), 2.49–2.38 (m, 2H), 2.27 (d, *J* = 13.9 Hz, 2H), 2.08–2.03 (m, 2H), 1.89–1.84 (m, 2H), 1.53 (s, 3H), 1.32 (s, 12H). ^{13}C NMR (101 MHz, $CDCl_3$): δ = 162.53, 161.46, 157.36, 150.29, 136.64, 133.25, 128.36, 116.32, 113.91, 106.87, 83.71, 65.79, 56.98, 55.43, 51.96, 49.66, 35.81, 26.43, 24.97. The signal of *C*-Bpin was not observed. LRMS (ESI) *m/z*: $[M+H]^+$ calculated for $C_{29}H_{41}BN_3O_7^+$: 554.30; found: 554.34. HRMS (ESI) *m/z*: $[M+H]^+$ calculated for $C_{29}H_{41}BN_3O_7^+$: 554.30321; found: 554.30247. Correct isotopic pattern.

4-Amino-2-methoxy-*N*-(4-methyl-1-{3-[4-(4,4,5,5-tetramethyl-1,3,2-dioxaborolan-2-yl)phenoxy]-propyl}piperidin-4-yl)benzamide (1) [51]**: 1** (0.9 g, 1.7 mmol, 90%, colorless oil or foam) was prepared from **6b** (1.04 g, 1.88 mmol, 1 eq.), pulverized Zn (1.23 g, 18.8 mmol, 10 eq.) and NH_4Cl (1.00 g, 18.8 mmol, 10 eq.) in 50% EtOH in EtOAc (50 mL) using the same procedure as described for R91150 except that the reaction time was increased to 24 h. The crude product was purified by column chromatography (SiO_2 with 0.1% Ca, $CHCl_3$/MeOH, 11:1). ^{1}H NMR (400 MHz, $CDCl_3$): δ = 7.94 (d, *J* = 8.5 Hz, 1H), 7.72 (d, *J* = 8.6 Hz, 2H), 7.59 (s, 1H), 6.85 (d, *J* = 8.6 Hz, 2H), 6.34 (dd, *J* = 8.5, 2.1 Hz, 1H), 6.20 (d, *J* = 2.0 Hz, 1H), 4.03 (t, *J* = 6.0 Hz, 4H), 3.90 (s, 3H), 3.01–2.89 (m, 2H), 2.79–2.69 (m, 2H), 2.51 (t, *J* = 10.6 Hz, 2H), 2.31 (d, *J* = 13.8 Hz, 2H), 2.13–2.02 (m, 2H), 1.84 (t, *J* = 11.1 Hz, 2H), 1.50 (s, 3H), 1.32 (s, 12H). ^{13}C NMR (101 MHz, $CDCl_3$): δ = 165.05, 161.40, 158.96, 151.07, 136.64, 133.72, 113.90, 112.61, 107.88, 97.37, 83.69, 65.72, 55.95, 55.44, 50.86, 49.66, 35.68, 26.58, 26.13, 24.97. The signal of *C*-Bpin was not observed. LRMS (ESI) *m/z*: $[M+H]^+$ calculated for $C_{29}H_{43}BN_3O_5^+$: 524.33; found: 524.25. HRMS (ESI) *m/z*: $[M+H]^+$ calculated for $C_{29}H_{43}BN_3O_5^+$: 524.32903; found: 524.32865. Correct isotopic pattern.

Benzyl 4-amino-4-methylpiperidine-1-carboxylate (11) [83]**:**

a) Benzyl 4-[(tert-butoxycarbonyl)amino]-4-methylpiperidine-1-carboxylate

Cbz-Cl (3.9 mL, 4.8 g, 28 mmol, 1.2 eq.) was added dropwise to K_2CO_3 (9.7 g, 70 mmol, 3 eq.) suspended in a solution of **4** (5.0 g, 23 mmol, 1 eq.) in anhydrous THF (117 mL). The reaction mixture was stirred at ambient temperature for 1.5 h, after which H_2O (117 mL) was added and the reaction mixture stirred for another 20 min. The aqueous phase was separated and extracted with EtOAc (3 × 150 mL). The combined organic phases were washed with sat. $NaHCO_3$ (2 × 100 mL), dried and concentrated under reduced pressure. The residue was purified by column chromatography (cyclohexane/EtOAc, 9:1) to afford benzyl 4-[(*tert*-butoxycarbonyl)amino]-4-methylpiperidine-1-carboxylate (8.1 g, 23 mmol, >99%) as a colorless oil, which gradually solidified to a colorless solid. R_f = 0.22 (cyclohexane/EtOAc, 9:1). ^{1}H NMR (400 MHz, $CDCl_3$): δ = 7.38–7.30 (m, 5H), 5.12 (s, 2H), 4.35 (s, 1H), 3.83–3.68 (m, 2H), 3.26–3.19 (m, 2H), 2.06–1.91 (m, 2H), 1.54–1.48 (m, 2H), 1.43 (s, 9H), 1.34 (s, 3H). ^{13}C NMR (101 MHz, $CDCl_3$): δ = 155.40, 136.94, 128.60, 128.09, 127.98, 127.09, 67.18, 50.59, 40.05, 36.20, 28.54, 27.03, 26.26. LRMS (ESI) *m/z*: $[M+H]^+$ calculated for $C_{19}H_{29}N_2O_4^+$: 349.21; found: 349.14. HRMS (ESI) *m/z*: $[M+Na]^+$ calculated for $C_{19}H_{29}N_2O_4Na^+$: 371.19413; found: 371.19387.

b) Benzyl 4-amino-4-methylpiperidine-1-carboxylate (**11**)

Benzyl 4-[(*tert*-butoxycarbonyl)amino]-4-methylpiperidine-1-carboxylate (8.1 g, 23 mmol, 1 eq.) was taken up into 20% TFA in CH_2Cl_2 (47 mL) and stirred for 16 h at ambient temperature. The reaction mixture was cooled to 0 °C, and saturated $NaHCO_3$ (100 mL) was slowly added. The mixture was allowed to warm up to ambient temperature and stirred for 10 min, after which the aqueous phase was separated and extracted with Et_2O (3 × 150 mL). The combined organic phases were dried over Na_2SO_4 and concentrated under reduced pressure to afford **11** (4.3 g, 17 mmol, 75%) as a colorless solid. ^{1}H NMR (400 MHz, $CDCl_3$): δ = 7.37–7.28 (m, 5H), 6.92–6.10 (br, 2H), 5.10 (s, 2H), 3.83–3.80 (m, 2H), 3.27–3.22 (m, 2H), 1.78–1.69 (m, 4H), 1.37 (s, 3H). ^{13}C NMR (101 MHz, $CDCl_3$): δ = 155.23, 136.53, 128.67, 128.26, 128.00, 67.58, 52.58, 39.84, 35.33, 23.13. LRMS (ESI) *m/z*: $[M+H]^+$ calculated for $C_{14}H_{21}N_2O_2^+$: 249.16; found: 249.10. HRMS (ESI) *m/z*: $[M+H]^+$ calculated for $C_{14}H_{21}N_2O_2^+$: 249.15975; found: 249.15980.

4-[(*tert*-Butoxycarbonyl)amino]-2-methoxybenzoic acid (12) [50]**:**

Boc_2O (9.6 mL, 9.8 g, 45 mmol, 1.5 eq.) was added (in one portion) to a solution of 4-aminobenzoic acid (5.0 g, 30 mmol, 1 eq.) and Et_3N (5.0 mL, 3.6 g, 36 mmol, 1.2 eq.) in MeOH (40 mL) and the reaction mixture was stirred at room temperature for 16 h. The solvent was removed under reduced pressure and the residue was dissolved in EtOAc. The resulting solution was washed with 10% citric acid, the EtOAc was removed under reduced pressure and the product crystalized in cyclohexane/EtOAc (2:1, 78 mL/g) to afford the title compound (3.9 g, 15 mmol, 49%, purity: >99%) as a colorless solid. The volume of the mother liquor was then reduced by half to afford, after crystallization, a second crop of **12** (1.05 g, 3.34 mmol, 11%, purity: 85%). R_f = 0.29 ($CHCl_3$/MeOH, 49:1). ^{1}H NMR [400 MHz, $(CD_3)_2SO$]: δ = 12.16 (br, 1H), 9.65 (s, 1H), 7.63 (d, *J* = 8.5 Hz, 1H), 7.35 (d, *J* = 1.8 Hz, 1H), 7.04 (dd, *J* = 8.6, 1.9, 1H), 3.76 (s, 3H), 1.48 (s, 9H). ^{13}C NMR [101 MHz, $(CD_3)_2SO$]: δ = 166.44, 159.67, 152.53, 144.63, 132.40, 113.48, 109.22, 101.40, 79.70, 55.48, 28.06. LRMS (ESI) *m/z*: $[M+H]^+$ calculated for $C_{13}H_{18}NO_5^+$: 268.12; found: 268.11. HRMS (ESI) *m/z*: $[M+H]^+$ calculated for $C_{13}H_{18}NO_5^+$: 268.11795; found: 268.11829.

2,3,5,6-Tetrafluorophenyl 4-[(*tert*-butoxycarbonyl)amino]-2-methoxybenzoate (13):

EDC (186 mg, 0.97 mmol, 1.3 eq.) was added to an ice-cold solution of **12** (200 mg, 0.75 mmol, 1 eq.) and 2,3,5,6-tetrafluorophenol (260 mg, 1.57 mmol, 2.1 eq.) in anhydrous CH_2Cl_2 (7.5 mL), and the mixture was stirred at ambient temperature for 16 h. The resulting dark red solution was diluted with CH_2Cl_2 and washed with H_2O (3 × 15 mL) and brine (3 × 15 mL). The organic phase was dried and concentrated under reduced pressure. The crude was product was purified by column

chromatography (cyclohexane/EtOAc, 9:1) to afford the title compound (187 mg, 0.45 mmol, 60%) as a colorless solid. ^{1}H NMR (400 MHz, $CDCl_3$): δ = 8.06 (d, *J* = 8.6 Hz, 1H), 7.51 (d, *J* = 7.51 Hz, 1H), 6.99 (m, 1H), 6.75 (dd, *J* = 8.6, 2.0 Hz, 2H), 3.96 (s, 3H), 1.54 (s, 9H). ^{13}C NMR (101 MHz, $CDCl_3$): δ = 162.58, 160.38, 151.95, 147.46–147.15 (m), 145.59, 144.96–144.69 (m), 142.37–142.07 (m), 139.89–139.68 (m), 144.84 (m), 139.89 (m), 134.15, 109.67, 109.31, 102.28 (t, *J* = 22.9 Hz), 101.26, 81.65, 56.13, 28.26. ^{19}F NMR (376 MHz, $CDCl_3$): δ = −139.59 (dd, *J* = 22.2, 9.7 Hz, 2F), −152.70 (dd, J = 22.2, 9.7, 2F). LRMS (ESI) *m/z*: $[M+H]^+$ calculated for $C_{19}H_{18}F_4NO_5^+$: 416.10; found: 416.03.

Benzyl 4-{4-[(*tert*-butoxycarbonyl)amino]-2-methoxybenzamido}-4-methylpiperidine-1-carboxylate (14):

Method A: HATU (4.98 g, 6.57 mmol, 1.5 eq.) was added in small portions to an ice-cold solution of **12** (1.76 g, 6.57 mmol, 1.5 eq.) and DIPEA (2.20 mL, 1.69 g, 13.1 mmol, 3 eq.) in anhydrous DMF (59 mL) and the mixture was stirred for 20 min. A solution of **11** (1.09 g, 4.37 mmol, 1 eq.) in anhydrous DMF (6.6 mL) was added dropwise to the resulting dark yellow solution and the reaction mixture was stirred at ambient temperature for 4 h. Ethylenediamine (1.5 mL) was then added and stirring was continued for 16 h, after which 1 M NaOH (50 mL) was added and the mixture stirred for another 15 min. The reaction mixture was diluted with H_2O (250 mL) and extracted with EtOAc (3 × 200 mL). The combined organic phases were washed with 1 M NaOH (200 mL), 0.5 M HCl (3 × 200 mL) and brine (3 × 200 mL), dried and concentrated under reduced pressure. The residue was purified by column chromatography (cyclohexane/EtOAc, 2:1, R_f = 0.20) to afford the title compound (1.07 g, 2.14 mmol, 49%) as a colorless solid.

Method B: A solution of **13** (199 mg, 0.48 mmol, 1 eq.), **11** (172 mg, 0.69 mmol, 1.4 eq.) and DIPEA (127 μL, 171 mg, 1.32 mmol, 3 eq.) in anhydrous DMA (4.4 mL) was stirred at 60 °C for 16 h. The reaction mixture was diluted with H_2O (50 mL) and extracted with EtOAc (3 × 50 mL). The combined organic phases were washed with 0.5 M NaOH (3 × 50 mL), 0.5 M HCl (3 × 50 mL) and brine (3 × 50 mL), and dried over Na_2SO_4. The solvent was removed under reduced pressure to afford the title compound (233 mg, 0.47 mmol, 98%) as a colorless solid.

^{1}H NMR [400 MHz, $(CD_3)_2SO$]: δ = 8.04 (d, *J* = 8.5 Hz, 1H), 7.76 (s, 1H), 7.54 (s, 1H), 7.36–7.29 (m, 5H), 6.73 (s, 1H), 6.68 (dd, *J* = 8.6, 2.0 Hz, 1H), 5.13 (s, 2H), 3.06 (s, 3H), 3.17 (t, *J* = 13.9 Hz, 2H), 2.26–2.16 (m, 2H), 1.68–1.57 (m, 4H), 1.52 (s, 9H), 1.51 (s, 3H). ^{13}C NMR [101 MHz, $(CD_3)_2SO$]: δ = 164.45, 158.34, 155.47, 152.41, 142.81, 136.95, 132.71, 128.62, 128.12, 128.01, 116.74, 110.59, 101.06, 81.29, 67.22, 56.26, 51.65, 40.16, 29.83, 28.43, 26.44. LRMS (ESI) *m/z*: $[M+H]^+$ calculated for $C_{27}H_{36}N_3O_6^+$: 498.26; found: 498.14.

4-[(*tert*-Butoxycarbonyl)amino]-2-methoxy-*N*-(4-methyl-1-{3-[4-(4,4,5,5-tetramethyl-1,3,2-dioxaborolan-2-yl)phenoxy]propyl}piperidin-4-yl)benzamide (10) [51]**:**

a) 4-[(tert-Butoxycarbonyl)amino]-2-methoxy-N-(4-methyl-piperidine-4-yl)benzamide

10% Pd/C (107 mg, w/w) was added to a solution **14** (1.07 g, 2.14 mmol, 1 eq.) in anhydrous MeOH (10 mL) and the reaction mixture was stirred in a hydrogen atmosphere for 16 h. The mixture was filtered through Celite® and concentrated under reduced pressure to afford 4-[(*tert*-butoxycarbonyl)amino]-2-methoxy-*N*-(4-methyl-piperidine-4-yl) benzamide (726 mg, 2.00 mmol, 93%) as a colorless solid, which was used for the next step without further purification. ^{1}H NMR [400 MHz, $(CD_3)_2SO$]: δ = 9.62 (s, 1H), 7.69 (s, 1H), 7.65 (d, *J* = 8.6 Hz, 1H), 7.38 (d, *J* = 1.4 Hz, 1H), 7.06 (dd, *J* = 8.5, 1.7 Hz, 1H), 3.87 (s, 3H), 2.87–2.83 (m, 2H), 2.77–2.71 (m, 2H), 2.14 (d, *J* = 13.4 Hz, 2H), 1.54–1.48 (m, 11H), 1.37 (s, 3H).

b) 4-[(tert-Butoxycarbonyl)amino]-2-methoxy-N-(4-methyl-1-{3-[4-(4,4,5,5-tetramethyl-1,3,2-dioxaborolan-2-yl)phenoxy]propyl}piperidin-4-yl)benzamide (**10**)

K_2CO_3 (1.00 g, 7.25 mmol, 3.7 eq.) and KI (3.26 g, 19.6 mmol, 10 eq.) were added to a solution of 4-[(*tert*-butoxycarbonyl)amino]-2-methoxy-*N*-(4-methyl-piperidine-4-yl)benzamide in anhydrous DMF (5 mL). **3b** (675 mg, 1.98 mmol, 1.01 eq.) was added in one portion to the resulting suspension and the reaction mixture was stirred for 4 h, after which H_2O (30 mL) followed by EtOAc (30 mL) were added. The organic phase was removed and the aqueous phase extracted with EtOAc (3 × 45 mL). The combined organic phases were washed with 0.1 M HCl (3 × 70 mL) and brine (3 × 70 mL), dried and concentrated under reduced pressure. The residue was purified by column chromatography ($CHCl_3$/MeOH, 19:1, R_f = 0.32) to afford **10** (864 mg, 1.39 mmol, 70%) as a colorless solid. ^{1}H NMR (400 MHz, $CDCl_3$): δ = 8.01 (d, *J* = 8.5 Hz, 1H), 7.71 (d, *J* = 8.7 Hz, 2H), 7.60 (d, *J* = 30.1 Hz, 2H), 6.83 (d, *J* = 8.5 Hz, 3H), 6.71 (dd, *J* = 8.7, 2.0 Hz, 1H), 4.05 (t, *J* = 5.8 Hz, 2H), 3.98 (s, 3H), 3.27–3.06 (m, 2H), 3.01–2.85 (m, 2H), 2.81–2.57 (m, 2H), 2.43 (d, *J* = 14.5 Hz, 2H), 2.34–2.23 (m, 2H), 2.21–2.09 (m, *J* = 10.1 Hz, 2H), 1.53 (s, 3H), 1.52 (s, 9H), 1.32 (s, 12H). ^{13}C NMR (101 MHz, $CDCl_3$): δ = 164.78, 161.12, 158.29, 152.40, 143.08, 136.68, 132.70, 116.40, 113.83, 110.71, 101.13, 83.72, 81.35, 65.26, 56.36, 55.27, 50.76, 49.36, 34.54, 28.41, 25.15, 24.96. The signal of *C*-Bpin was not observed. LRMS (ESI) *m/z*: $[M+H]^+$ calculated for $C_{34}H_{51}BN_3O_7^+$: 624.37; found: 624.32. Correct isotopic pattern.

3.2. Radiochemistry

3.2.1. General conditions

[^{18}F]Fluoride ([^{18}F]F^-) was produced via the $^{18}O(p,n)^{18}F$ nuclear reaction by bombardment of enriched [^{18}O]H_2O with 16.5 MeV protons using a BC1710 cyclotron (The Japan Steel Works Ltd., Shinagawa, Japan) at the INM-5 (Forschungszentrum Jülich). All radiosyntheses were carried out in 5 mL Wheaton V-Vials equipped with PTFE-coated wing stir bars. Anhydrous solvents (DMI, *n*BuOH and MeOH, dried over molecular sieves) were purchased from Sigma-Aldrich (Steinheim, Germany). Anion exchange resins (Sep-Pak Accell Plus QMA carbonate plus light cartridges with 40 mg sorbent per cartridge) were obtained from Waters (Eschborn, Germany) and polymeric-based StrataX cartridges (60 mg) were obtained from Phenomenex (Aschaffenburg, Germany).

3.2.2. Processing of [^{18}F]F^-

Aqueous [^{18}F]F^- was loaded (from the female side) onto a QMA cartridge (preconditioned with 1 mL H_2O) and the cartridge was washed (from the male side) with anhydrous MeOH (1 mL) to remove residual H_2O and dried (from the female side) with air (2 × 10 mL). [^{18}F]F^- was eluted (from the female to the male side) with a solution of Et_4NOTf in MeOH (500 μL), and the MeOH was evaporated at 80 °C under reduced pressure in a stream of argon to give Et_4N[^{18}F]F/Et_4NOTf, which was used for the radiosyntheses as described below.

3.2.3. High-performance liquid chromatography (HPLC)

Analytical radio-HPLC was performed on a HPLC system (Knauer Wissenschaftliche Geräte GmbH, Berlin, Germany) with Azura P 6.1L pump and Azura UVD 2.1S UV/Vis detector. For monitoring UV absorbance and radioactivity, the UV/Vis detector was coupled in series with a Berthold NaI detector, giving a time of delay of 0.1–0.3 min (depending on the flow rate) between the corresponding responses. Alternatively, an Ultimate® 3000 HPLC system with Ultimate® 3000 LPG-3400A pump and an Ultimate® 3000 VWD-3100 UV/Vis detector (Thermo Fisher Scientific, Langerwehe, Germany) coupled in series with a Gabi Star γ-detector (Raytest GmbH, Straubenhardt, Germany) was used. To avoid errors due to adsorption processes on the stationary phase, radiochemical conversions (RCCs) and radiochemical purities (RCPs) were determined by radio-HPLC with post-column injection (for details see Ref. [84]) after dilution of the reaction mixtures with H_2O (1 mL) or 20% MeCN (1 mL). Radio-HPLC traces were not decay-corrected and radiochemical conversions are given as non-decay-corrected RCCs. For determination of RCPs, the integrals of the peaks of post-column injections were manually decay-corrected to the integrals of the product peaks. The identity of radiolabeled products was confirmed by

co-injection of the corresponding non-radiolabeled reference compound. Activity yields (AY) were determined as the ratio between the activity of the purified radiolabeled product and the initial activity of [^{18}F]F$^-$ on the QMA cartridge.

Purification of crude [^{18}F]R91150 by semipreparative HPLC was performed with a dedicated HPLC system consisting of a Knauer pump 40P, a Knauer K-2500 detector, a Rheodyne 6-way valve and a Geiger-Müller counter.

3.2.4. Analytical HPLC conditions

[^{18}F]R91150 prepared from **1**: Column: MultoKrom® 100-5, 5 μm, 250 × 4.6 mm (CS-Chromatography Service GmbH, Langerwehe, Germany); eluent: 30% MeCN (0.1% TFA); flow rate: 1.3 mL/min; t_R = 7.85 min.

Boc-[^{18}F]R91150 prepared from **10**: Column: MultoKrom® 100-5, 5 μm, 250 × 4.6 mm (CS-Chromatography Service GmbH, Langerwehe, Germany); eluent: 50% MeCN (0.1% TFA); flow rate: 1.5 mL/min; t_R = 4.62 min.

3.2.5. Preparative HPLC conditions

Column: Gemini C18 110A, 5 μm, 250 × 10 mm (Phenomenex Ltd, Aschaffenburg, Germany); eluent: 25% MeCN in 25 mM sodium acetate buffer (pH = 5.18); flow rate: 7.1 mL/min; t_R = 18–21 min.

3.2.6. Quality control

For [^{18}F]R91150 prepared from **1**: Column: Kinetex EVO C18, 5 μm, 250 × 4.6 mm (Phenomenex Ltd, Aschaffenburg, Germany); eluent: 20% MeCN (0.1% TFA), flow rate: 1.0 mL, t_R = 9.55 min.

For [^{18}F]R91150 prepared from **10**: Column: MultoKrom® 100-5 C18, 5 μm, 250 × 4.6 mm (CS-Chromatography Service GmbH, Langerwehe, Germany); eluent: 30% MeCN (0.1% TFA); flow rate: 1.5 mL/min; t_R = 8.98 min.

The assessment of radioactivity retention on different stationary phases (see section 3 in the supporting information) was performed using a Kinetex EVO C18, 5 μm, 250 × 4.6 mm column (Phenomenex Ltd, Aschaffenburg, Germany), a Chromolith SpeedROD, RP-18e, 50 × 4.6 mm column (Merck KGaA, Darmstadt, Germany) or a Luna 5u HILIC, 250 × 4.60 mm, 5 μm column (Phenomenex, Aschaffenburg, Germany) as indicated and under the conditions (eluent, flow rate) specified in the respective figure.

3.2.7. Thin layer chromatography (TLC)

Radio-TLC was performed with Silica gel 60 RP-18 F_{254}S or Silica gel 60 F_{254} plates (both from Merck KGaA, Darmstadt, Germany). The chromatograms were visualized by a PerkinElmer Cyclone® Plus phosphor imaging system [PerkinElmer LAS (Germany) GmbH, Rodgau, Germany] using the OptiQuant 5.0 software. After development of the TLC plates, they were air-dried for 2–3 min and then covered with plastic foil before exposing them to the film.

3.2.8. Preparation of [^{18}F]R91150

*Preparation from **1** (from non-protected precursor).* Et_4N[^{18}F]F/Et_4NOTf (0.02–6.8 GBq) was taken up into a solution of **1** (2.6 mg, 5 μmol) and Cu(4-PhPy)$_4$(ClO$_4$)$_2$ (8.8 mg, 10 μmol) in DMI/*n*BuOH (2:1, 1.2 mL) and the reaction mixture was stirred under air at 110 °C for 10 min. The mixture was diluted with H_2O (19 mL) and loaded onto a StrataX cartridge. The cartridge was washed with H_2O (5 mL) and the crude radiolabeled product was eluted with MeCN (500 μL). The resulting solution was diluted with 25 mM sodium acetate buffer (pH = 5.18; 1 mL) and loaded onto a preparative HPLC column. The product fraction was collected at 18–21 min, diluted with H_2O (19 mL) and loaded onto a StrataX cartridge. The cartridge was washed with H_2O (5 mL) and the radiolabeled product was eluted with EtOH (600 μL). The resulting solution was concentrated to approximately 50 μL at 40 °C in a stream of argon under reduced pressure, and the residue was taken up into 2% Tween-80 (0.6 mL) to afford [^{18}F]F91150 as ready-to-inject solution.

*Preparation from **10** (from N-Boc-protected precursor).* Et_4N[^{18}F]F/Et_4NOTf (0.1–5.7 GBq) was taken up into a solution of **10** (6.2 mg, 10 μmol) and Cu(4-PhPy)$_4$(ClO$_4$)$_2$ (8.7 mg, 10 μmol) in DMI/*n*BuOH (2:1, 1.2 mL) and the reaction mixture was stirred under air at 110 °C for 10 min. The reaction mixture was diluted with H_2O (19 mL) and loaded onto a StrataX cartridge. The cartridge was washed with H_2O (5 mL) and the crude radiolabeled intermediate was eluted with MeOH (600 μL). The solvent was removed at 60 °C in a stream of argon under reduced pressure and 6 M HCl (500 μL) was added. The mixture was stirred at 80 °C for 10 min to deprotect the radiolabeled intermediate and then diluted with 6 M NaOH (350 μL) and H_2O (1 mL). [^{18}F]F91150 was isolated and formulated as described above.

3.3. In vivo experiments

3.3.1. Experimental animals

Animal experiments were carried out in accordance with the EU directive 2010/63/EU and the German Animal Welfare Act (TierSchG, 2006), and were approved by regional authorities (Ministry for Environment, Agriculture, Conservation and Consumer Protection of the State of North Rhine-Westphalia, license number 84-02.04.2017.A288). Nine healthy Long Evans rats (females; 300–578 g) and four healthy C57BL/6 mice (females, 18–20 g) were used for this study. Animals were housed in groups of 2–4 in individually ventilated cages (NexGen Ecoflo, Allentown Inc., Allentown, NJ, USA) under controlled ambient conditions (22 ± 1 °C and 55 ± 5% relative humidity). Food and water were available *ad libitum*.

3.3.2. In vivo PET experiments

Prior to PET measurements, animals were anesthetized with isoflurane in O_2/air (3:7) [5% for induction, 1.5–2.5% for maintenance], and a catheter for tracer injection was inserted into the lateral tail vein. Animals were placed on an animal holder (Equipment Vétérinaire Minerve, Esternay, France for rats, and Medres, Cologne for mice), and fixed with a tooth bar in a respiratory mask. PET scans in list mode were performed using a Focus 220 micro PET scanner (CTI-Siemens, Germany) with a resolution at the center of field of view of 1.4 mm. Data acquisition started with injection of the tracer (54.2 ± 8.2 MBq [^{18}F]F91150 in 500 μL for rats and 9.5 ± 0.9 MBq in 125 μL for mice), continued for 120 min and was followed by a 10 min transmission scan using a ^{57}Co point source. Breathing rate was monitored and maintained at around 60/min by adjusting the isoflurane concentration (1.5–2.5%). Body temperature was maintained at 37 °C by a feedback-controlled system. After the scan, the animals were returned to their home cage. For the heterologous blocking experiments, 1.5 mg/kg altanserin (n = 3 rats) or 0.1 mg/kg SB242084 (n = 4 rats) were administered by intraperitoneal (i.p.) injection 50 or 20 min before tracer injection, respectively. For the heterologous displacement experiments (n = 3 rats), 1.5 mg/kg ketanserin was administered by intravenous (i.v.) injection 60 min after tracer injection (i.e. in the middle of the 120 min PET measurements). For the homologous blocking experiments (n = 3 rats), 1 mg/kg non-labeled R91150 was administered by i.v. injection 5 min before tracer injection.

The emission scans were histogrammed into time frames (2 × 1 min, 2 × 2 min, 6 × 4 min, 18 × 5 min for time-activity curves, and 4 × 30 min for display) and fully 3D rebinned (span 3, ring difference 47), followed by OSEM3D/MAP reconstruction. The resulting voxel sizes were 0.38 × 0.38 × 0.80 mm^3 for rats, and 0.47 × 0.47 × 0.80 mm^3 for mice. Postprocessing and image analysis was performed with VINCI 5.21 (Max-Planck-Institute for Metabolism Research, Cologne, Germany). Images were intensity-normalized to injected dose and corrected for body weight (SUV_{bw}). To this end, every frame was divided by injected dose and multiplied by body weight.

CRediT authorship contribution statement

Chris Hoffmann: Writing – review & editing, Writing – original draft, Investigation, Formal analysis. **Heike Endepols:** Writing – review & editing, Writing – original draft, Visualization, Supervision, Investigation, Formal analysis, Conceptualization. **Elizaveta A. Urusova:** Writing – review & editing, Investigation. **Dominik Elchine:** Writing – review & editing, Investigation. **Felix Neumaier:** Writing – review & editing, Writing – original draft, Visualization, Investigation. **Bernd Neumaier:** Writing – review & editing, Supervision, Project administration, Funding acquisition, Conceptualization. **Boris D. Zlatopolskiy:** Writing – review & editing, Writing – original draft, Visualization, Supervision, Investigation, Funding acquisition, Formal analysis, Conceptualization.

Funding sources

This work was supported by Deutsche Forschungsgemeinschaft (DFG) grants ZL 65/1-1, ZL 65/3-1 and ZL 65/4-1.

Declaration of competing interest

The authors declare that they have no known competing financial interests or personal relationships that could have appeared to influence the work reported in this paper.

Acknowledgements

We thank Dmitrii Antuganov for his excellent technical assistance.

4 Abbreviations

[^{18}F]F$^-$, [^{18}F]fluoride; 5-HT, serotonin; A_m, molar activity; AY, activity yield; Cbz-Cl, benzyl chloroformate; CSF, cerebrospinal fluid; DIPEA, *N*,*N*-diisopropylethylamine; DMF, *N*,*N*-dimethylformamide; DMI, 1,3-dimethyl-2-imidazolidinone; EDC, 1-ethyl-3-(3-dimethylaminopropyl)carbodiimide hydrochloride; ESI, electrospray ionization; HATU, azabenzotriazole tetramethyluronium hexafluorophosphate; HPLC, high-performance liquid chromatography; HRMS, high resolution mass spectra; i.p., intraperitoneal; i.v., intravenous; LRMS, low resolution mass spectra; NMR, nuclear magnetic resonance; n.c.a., no-carrier-added; PET, positron emission tomography; RCC, radiochemical conversion; RCP, radiochemical purity; SPE, solid phase extraction; SPECT, single photon emission computed tomography; SUV_{bw}, standardized uptake value normalized by body weight; TFA, trifluoroacetic acid; THF, tetrahydrofuran; TIS, triisopropylsilane; TLC, thin layer chromatography; VOI, volume of interest.

Appendix A. Supplementary data

Supplementary data to this article can be found online at https://doi.org/10.1016/j.ejmech.2025.117265.

Data availability

Data will be made available on request.

References

[1] N.M. Barnes, G.P. Ahern, C. Becamel, J. Bockaert, M. Camilleri, S. Chaumont-Dubel, S. Claeysen, K.A. Cunningham, K.C. Fone, M. Gershon, G. Di Giovanni, N. M. Goodfellow, A.L. Halberstadt, R.M. Hartley, G. Hassaine, K. Herrick-Davis, R. Hovius, E. Lacivita, E.K. Lambe, M. Leopoldo, F.O. Levy, S.C.R. Lummis, P. Marin, L. Maroteaux, A.C. McCreary, D.L. Nelson, J.F. Neumaier, A. Newman-Tancredi, H. Nury, A. Roberts, B.L. Roth, A. Roumier, G.J. Sanger, M. Teitler, T. Sharp, C.M. Villalón, H. Vogel, S.W. Watts, D. Hoyer, International union of basic and clinical pharmacology. CX. Classification of receptors for 5-hydroxytryptamine; pharmacology and function, Pharmacol. Rev. 73 (2021) 310–520, https://doi.org/10.1124/pr.118.015552.

[2] J. Schmitt, M. Wingen, J. Ramaekers, E. Evers, W. Riedel, Serotonin and human cognitive performance, Curr. Pharmaceut. Des. 12 (2006) 2473–2486, https://doi.org/10.2174/138161206777698909.

[3] G. Zhang, R.W. Stackman, The role of serotonin 5-HT_{2A} receptors in memory and cognition, Front. Pharmacol. 6 (2015), https://doi.org/10.3389/fphar.2015.00225.

[4] M. Naughton, J.B. Mulrooney, B.E. Leonard, A review of the role of serotonin receptors in psychiatric disorders, Hum. Psychopharmacol. Clin. Exp. 15 (2000) 397–415, https://doi.org/10.1002/1099-1077(200008)15:6<397::AID-HUP212>3.0.CO;2-L.

[5] B. Dean, W. Hayes, Decreased frontal cortical serotonin2A receptors in schizophrenia, Schizophr. Res. 21 (1996) 133–139, https://doi.org/10.1016/0920-9964(96)00034-5.

[6] J.J. Rodríguez, H.N. Noristani, A. Verkhratsky, The serotonergic system in ageing and Alzheimer's disease, Prog. Neurobiol. 99 (2012) 15–41, https://doi.org/10.1016/j.pneurobio.2012.06.010.

[7] E.K. Perry, R.H. Perry, J.M. Candy, A.F. Fairbairn, G. Blessed, D.J. Dick, B. E. Tomlinson, Cortical serotonin-S2 receptor binding abnormalities in patients with Alzheimer's disease: comparisons with Parkinson's disease, Neurosci. Lett. 51 (1984) 353–357, https://doi.org/10.1016/0304-3940(84)90402-6.

[8] M.K. Lai, S.W. Tsang, J.T. Alder, J. Keene, T. Hope, M.M. Esiri, P.T. Francis, C. P. Chen, Loss of serotonin 5-HT_{2A} receptors in the postmortem temporal cortex correlates with rate of cognitive decline in Alzheimer's disease, Psychopharmacology (Berl) 179 (2005) 673–677, https://doi.org/10.1007/s00213-004-2077-2.

[9] L. Santhosh, K.M. Estok, R.S. Vogel, G.D. Tamagnan, R.M. Baldwin, E.M. Mitsis, M. G. MacAvoy, J.K. Staley, C.H. van Dyck, Regional distribution and behavioral correlates of 5-HT_{2A} receptors in Alzheimer's disease with [^{18}F]deuteroaltanserin and PET, Psychiatry Res. Neuroimaging. 173 (2009) 212–217, https://doi.org/10.1016/j.pscychresns.2009.03.007.

[10] J. Blin, J.C. Baron, B. Dubois, C. Crouzel, M. Fiorelli, D. Attar-Lévy, B. Pillon, D. Fournier, M. Vidailhet, Y. Agid, Loss of brain 5-HT_2 receptors in Alzheimer's disease. In vivo assessment with positron emission tomography and [^{18}F] setoperone, Brain 116 (1993) 497–510, https://doi.org/10.1093/brain/116.3.497.

[11] J. Versijpt, K.J. Van Laere, F. Dumont, D. Decoo, M. Vandecapelle, P. Santens, I. Goethals, K. Audenaert, G. Slegers, R.A. Dierckx, J. Korf, Imaging of the 5-HT_{2A} system: age-, gender-, and Alzheimer's disease-related findings, Neurobiol. Aging 24 (2003) 553–561, https://doi.org/10.1016/S0197-4580(02)00137-9.

[12] J.H. Meyer, S. McMain, S.H. Kennedy, L. Korman, G.M. Brown, J.N. DaSilva, A. A. Wilson, T. Blak, R. Eynan-Harvey, V.S. Goulding, S. Houle, P. Links, Dysfunctional attitudes and 5-HT_2 receptors during depression and self-harm, Am. J. Psychiatr. 160 (2003) 90–99, https://doi.org/10.1176/appi.ajp.160.1.90.

[13] Z. Bhagwagar, R. Hinz, M. Taylor, S. Fancy, P. Cowen, P. Grasby, Increased 5-HT_{2A} receptor binding in euthymic, medication-free patients recovered from depression: a positron emission study with [^{11}C]MDL 100,907, Am. J. Psychiatr. 163 (2006) 1580–1587, https://doi.org/10.1176/ajp.2006.163.9.1580.

[14] W. Kroeze, B. Roth, The molecular biology of serotonin receptors: therapeutic implications for the interface of mood and psychosis, Biol. Psychiatr. 44 (1998) 1128–1142, https://doi.org/10.1016/S0006-3223(98)00132-2.

[15] H. Meltzer, The role of serotonin in antipsychotic drug action, Neuropsychopharmacology 21 (1999) 106S–115S, https://doi.org/10.1016/S0893-133X(99)00046-9.

[16] H. Cohen, Anxiolytic effect and memory improvement in rats by antisense oligodeoxynucleotide to 5-hydroxytryptamine-2A precursor protein, Depress. Anxiety 22 (2005) 84–93, https://doi.org/10.1002/da.20087.

[17] R. Lewis, S. Kapur, C. Jones, J. DaSilva, G.M. Brown, A.A. Wilson, S. Houle, R. B. Zipursky, Serotonin 5-HT_2 receptors in schizophrenia: a PET study using [^{18}F] setoperone in neuroleptic-naive patients and normal subjects, Am. J. Psychiatr. 156 (1999) 72–78, https://doi.org/10.1176/ajp.156.1.72.

[18] Y. Okubo, T. Suhara, K. Suzuki, K. Kobayashi, O. Inoue, O. Terasaki, Y. Someya, T. Sassa, Y. Sudo, E. Matsushima, M. Iyo, Y. Tateno, T. Michi, Serotonin 5-HT_2 receptors in schizophrenic patients studied by positron emission tomography, Life Sci. 66 (2000) 2455–2464, https://doi.org/10.1016/S0024-3205(00)80005-3.

[19] C. Trichard, M.-L. Paillère-Martinot, D. Attar-Levy, J. Blin, A. Feline, J.-L. Martinot, No serotonin 5-HT_{2A} receptor density abnormality in the cortex of schizophrenic patients studied with PET, Schizophr. Res. 31 (1998) 13–17, https://doi.org/10.1016/S0920-9964(98)00014-0.

[20] E.T.C. Ngan, L.N. Yatham, T.J. Ruth, P.F. Liddle, Decreased serotonin 2A receptor densities in neuroleptic-naive patients with schizophrenia: a PET study using [^{18}F] setoperone, Am. J. Psychiatr. 157 (2000) 1016–1018, https://doi.org/10.1176/appi.ajp.157.6.1016.

[21] H. Rasmussen, D. Erritzoe, R. Andersen, B.H. Ebdrup, B. Aggernaes, B. Oranje, J. Kalbitzer, J. Madsen, L.H. Pinborg, W. Baaré, C. Svarer, H. Lublin, G.M. Knudsen, B. Glenthoj, Decreased frontal Serotonin2A receptor binding in antipsychotic-naive patients with first-episode schizophrenia, Arch. Gen. Psychiatr. 67 (2010) 9, https://doi.org/10.1001/archgenpsychiatry.2009.176.

[22] C. Lemaire, R. Cantineau, M. Guillaume, A. Plenevaux, L. Christiaens, Fluorine-18-altanserin: a radioligand for the study of serotonin receptors with PET: radiolabeling and in vivo biologic behavior in rats, J. Nucl. Med. 32 (1991) 2266–2272. http://www.ncbi.nlm.nih.gov/pubmed/1744713.

[23] C.C. Meltzer, G. Smith, J.C. Price, C.F. Reynolds, C.A. Mathis, P. Greer, B. Lopresti, M.A. Mintun, B.G. Pollock, D. Ben-Eliezer, M.N. Cantwell, W. Kaye, S.T. DeKosky, Reduced binding of [^{18}F]altanserin to serotonin type 2A receptors in aging:

persistence of effect after partial volume correction, Brain Res. 813 (1998) 167–171, https://doi.org/10.1016/S0006-8993(98)00909-3.
[24] L.H. Pinborg, K.H. Adams, S. Yndgaard, S.G. Hasselbalch, S. Holm, H. Kristiansen, O.B. Paulson, G.M. Knudsen, [^{18}F]Altanserin binding to human 5HT$_{2A}$ receptors is unaltered after citalopram and pindolol challenge, J. Cerebr. Blood Flow Metabol. 24 (2004) 1037–1045, https://doi.org/10.1097/01.WCB.0000126233.08565.E7.
[25] G. Pauwelyn, L. Vlerick, R. Dockx, J. Verhoeven, A. Dobbeleir, T. Bosmans, K. Peremans, C. Vanhove, I. Polis, F. De Vos, Kinetic analysis of [^{18}F]altanserin bolus injection in the canine brain using PET imaging, BMC Vet. Res. 15 (2019) 415, https://doi.org/10.1186/s12917-019-2165-5.
[26] J. Blin, G. Sette, M. Fiorelli, O. Bletry, J.L. Elghozi, C. Crouzel, J.C. Baron, A method for the in vivo investigation of the serotonergic 5-HT$_2$ receptors in the human cerebral cortex using positron emission tomography and ^{18}F-labeled setoperone, J. Neurochem. 54 (1990) 1744–1754, https://doi.org/10.1111/j.1471-4159.1990.tb01229.x.
[27] D.Q. Beversdorf, R.E. Nordgren, A.A. Bonab, A.J. Fischman, S.B. Weise, D. D. Dougherty, G.J. Felopulos, F.C. Zhou, M.L. Bauman, 5-HT$_2$ receptor distribution shown by [^{18}F]setoperone PET in high-functioning autistic adults, J. Neuropsychiatry Clin. Neurosci. 24 (2012) 191–197, https://doi.org/10.1176/appi.neuropsych.11080202.
[28] J.H. Meyer, S. Kapur, S. Houle, J. DaSilva, B. Owczarek, G.M. Brown, A.A. Wilson, S.H. Kennedy, Prefrontal cortex 5-HT$_2$ receptors in depression: an [^{18}F]setoperone PET imaging study, Am. J. Psychiatr. 156 (1999) 1029–1034, https://doi.org/10.1176/ajp.156.7.1029.
[29] D. Attar-Lévy, J.-L. Martinot, J. Blin, M.-H. Dao-Castellana, C. Crouzel, B. Mazoyer, M.-F. Poirier, M.-C. Bourdel, N. Aymard, A. Syrota, A. Féline, The cortical serotonin2 receptors studied with positron-emission tomography and [^{18}F]-setoperone during depressive illness and antidepressant treatment with clomipramine, Biol. Psychiatr. 45 (1999) 180–186, https://doi.org/10.1016/S0006-3223(98)00007-9.
[30] H. Ito, S. Nyberg, C. Halldin, C. Lundkvist, L. Farde, PET imaging of central 5-HT$_{2A}$ receptors with carbon-11-MDL 100,907, J. Nucl. Med. 39 (1998) 208–214. http://www.ncbi.nlm.nih.gov/pubmed/9443763.
[31] H.B. Simpson, M. Slifstein, J. Bender, X. Xu, E. Hackett, M.J. Maher, A. Abi-Dargham, Serotonin 2A receptors in obsessive-compulsive disorder: a positron emission tomography study with [^{11}C]MDL 100907, Biol. Psychiatr. 70 (2011) 897–904, https://doi.org/10.1016/j.biopsych.2011.06.023.
[32] P.-Z. Tan, R. Baldwin, C. Van Dyck, M. Al-Tikriti, B. Roth, N. Khan, D. Charney, R. Innis, Characterization of radioactive metabolites of 5-HT$_{2A}$ receptor PET ligand [^{18}F]altanserin in human and rodent, Nucl. Med. Biol. 26 (1999) 601–608, https://doi.org/10.1016/S0969-8051(99)00022-0.
[33] J.E. Leysen, Use of 5-HT receptor agonists and antagonists for the characterization of their respective receptor sites, in: Drugs as Tools Neurotransmitter Res., Humana Press, New Jersey, 1989, pp. 299–350, https://doi.org/10.1385/0-89603-122-5:299.
[34] J. Blin, S. Pappata, M. Kiyosawa, C. Crouzel, J.C. Baron, [^{18}F]Setoperone: a new high-affinity ligand for positron emission tomography study of the serotonin-2 receptors in baboon brain in vivo, Eur. J. Pharmacol. 147 (1988) 73–82, https://doi.org/10.1016/0014-2999(88)90635-8.
[35] U. Mühlhausen, J. Ermert, M.M. Herth, H.H. Coenen, Synthesis, radiofluorination and first evaluation of (±)-[^{18}F]MDL 100907 as serotonin 5-HT$_{2A}$ receptor antagonist for PET, J. Label. Compd. Radiopharm. 52 (2009) 6–12, https://doi.org/10.1002/jlcr.1563.
[36] H. Ren, H.-Y. Wey, M. Strebl, R. Neelamegam, T. Ritter, J.M. Hooker, Synthesis and imaging validation of [^{18}F]MDL100907 enabled by Ni-mediated fluorination, ACS Chem. Neurosci. 5 (2014) 611–615, https://doi.org/10.1021/cn500078e.
[37] L.N. Chavan, R. Voll, M.M. Sanchez, J.A. Nye, M.M. Goodman, Concise and scalable radiosynthesis of (+)-[^{18}F]MDL100907 as a serotonin 5-HT$_{2A}$ receptor antagonist for PET, ACS Chem. Neurosci. 14 (2023) 3694–3703, https://doi.org/10.1021/acschemneuro.3c00382.
[38] F. Debus, M.M. Herth, M. Piel, H.-G. Buchholz, N. Bausbacher, V. Kramer, H. Lüddens, F. Rösch, ^{18}F-Labeling and evaluation of novel MDL 100907 derivatives as potential 5-HT2A antagonists for molecular imaging, Nucl. Med. Biol. 37 (2010) 487–495, https://doi.org/10.1016/j.nucmedbio.2010.02.002.
[39] V. Kramer, A. Dyssegaard, J. Flores, C. Soza-Ried, F. Rösch, G.M. Knudsen, H. Amaral, M.M. Herth, Characterization of the serotonin 2A receptor selective PET tracer (R)-[^{18}F]MH.MZ in the human brain, Eur. J. Nucl. Med. Mol. Imag. 47 (2020) 355–365, https://doi.org/10.1007/s00259-019-04527-w.
[40] M.M. Herth, G.M. Knudsen, PET imaging of the 5-HT$_{2A}$ receptor system: a tool to study the receptor's in vivo brain function, in: 5-HT$_{2A}$ Recept. Cent. Nerv. Syst., Springer International Publishing, Cham, 2018, pp. 85–134, https://doi.org/10.1007/978-3-319-70474-6_5.
[41] U. Schmitt, D.E. Lee, M.M. Herth, M. Piel, H.-G. Buchholz, F. Roesch, C. Hiemke, H. Lueddens, F. Debus, P-glycoprotein influence on the brain uptake of a 5-HT$_{2A}$ ligand: [^{18}F]MH.MZ, Neuropsychobiology 63 (2011) 183–190, https://doi.org/10.1159/000321594.
[42] J. Mertens, D. Terriere, V. Sipido, W. Gommeren, P.M.F. Janssen, J.E. Leysen, Radiosynthesis of a new radioiodinated ligand for serotonin-5HT$_2$-receptors, a promising tracer for γ-emission tomography, J. Label. Compd. Radiopharm. 34 (1994) 795–806, https://doi.org/10.1002/jlcr.2580340902.
[43] D. Terriere, P.M.F. Janssen, W. Gommeren, M. Gysemans, J.J.R. Mertens, J. E. Leysen, Evaluation of radioiodo-4-amino-N-[1-[3-(4-fluorophenoxy)-propyl]-4-methyl-4-piperidinyl]-5-iodo-2-methoxybenzamide as a potential 5HT2 receptor tracer for SPE(C)T, Nucl. Med. Biol. 22 (1995) 1005–1010, https://doi.org/10.1016/0969-8051(95)02023-3.
[44] C. Baeken, R. De Raedt, A. Bossuyt, C. Van Hove, J. Mertens, A. Dobbeleir, P. Blanckaert, I. Goethals, The impact of HF-rTMS treatment on serotonin$_{2A}$ receptors in unipolar melancholic depression, Brain Stimul. 4 (2011) 104–111, https://doi.org/10.1016/j.brs.2010.09.002.
[45] S.T. Vermeire, K.R. Audenaert, A.A. Dobbeleir, R.H. De Meester, F.J. De Vos, K. Y. Peremans, Evaluation of the brain 5-HT2A receptor binding index in dogs with anxiety disorders, measured with ^{123}I-5I-R91150 and SPECT, J. Nucl. Med. 50 (2009) 284–289, https://doi.org/10.2967/jnumed.108.055731.
[46] K. Peremans, B. De Spiegeleer, E. Buntinx, A. Dobbeleir, S. Vermeire, E. Vandermeulen, F. De Vos, A. Megens, J. Eersels, K. Audenaert, Evaluation of serotonin-2A receptor occupancy with ^{123}I-5-I-R91150 and single-photon emission tomography before and after low-dose pipamperone administration in the canine brain, Nucl. Med. Commun. 29 (2008) 724–729, https://doi.org/10.1097/MNM.0b013e3282fdc989.
[47] K. Audenaert, K. Van Laere, F. Dumont, M. Vervaet, I. Goethals, G. Slegers, J. Mertens, C. van Heeringen, R.A. Dierckx, Decreased 5-HT$_{2a}$ receptor binding in patients with anorexia nervosa, J. Nucl. Med. 44 (2003) 163–169. http://www.ncbi.nlm.nih.gov/pubmed/12571204.
[48] M.J. Travis, G.F. Busatto, L.S. Pilowsky, R. Mulligan, P.D. Acton, S. Gacinovic, J. Mertens, D. Terrière, D.C. Costa, P.J. Ell, R.W. Kerwin, 5-HT$_{2A}$ receptor blockade in patients with schizophrenia treated with risperidone or clozapine, Br. J. Psychiatry 173 (1998) 236–241, https://doi.org/10.1192/bjp.173.3.236.
[49] M. Melse, S.K.H. Tan, Y. Temel, M.J.P.G. van Kroonenburgh, A.F.G. Leentjens, Changes in 5-HT$_{2A}$ Receptor Expression in Untreated, de novo Patients with Parkinson's Disease, J. Parkinsons Dis. 4 (2014) 283–287, https://doi.org/10.3233/JPD-130300.
[50] U. Mühlhausen, J. Ermert, H.H. Coenen, Synthesis, labelling and first evaluation of [^{18}F]R91150 as a serotonin 5-HT$_{2A}$ receptor antagonist for PET, J. Label. Compd. Radiopharm. 52 (2009) 13–22, https://doi.org/10.1002/jlcr.1565.
[51] M. Willmann, J. Hegger, B. Neumaier, J. Ermert, Radiosynthesis and biological evaluation of [^{18}F]R91150, a selective 5-HT$_{2A}$ receptor antagonist for PET-imaging, ACS Med. Chem. Lett. 12 (2021) 738–744, https://doi.org/10.1021/acsmedchemlett.0c00658.
[52] N. Ichiishi, A.F. Brooks, J.J. Topczewski, M.E. Rodnick, M.S. Sanford, P.J.H. Scott, Copper-catalyzed [^{18}F]fluorination of (Mesityl)(aryl)iodonium salts, Org. Lett. 16 (2014) 3224–3227, https://doi.org/10.1021/ol501243g.
[53] M. Tredwell, S.M. Preshlock, N.J. Taylor, S. Gruber, M. Huiban, J. Passchier, J. Mercier, C. Génicot, V. Gouverneur, A general copper-mediated nucleophilic ^{18}F fluorination of arenes, Angew. Chem. Int. Ed. 53 (2014) 7751–7755, https://doi.org/10.1002/anie.201404436.
[54] A.V. Mossine, A.F. Brooks, K.J. Makaravage, J.M. Miller, N. Ichiishi, M.S. Sanford, P.J.H. Scott, Synthesis of [^{18}F]arenes via the copper-mediated [^{18}F]fluorination of boronic acids, Org. Lett. 17 (2015) 5780–5783, https://doi.org/10.1021/acs.orglett.5b02875.
[55] K.J. Makaravage, A.F. Brooks, A.V. Mossine, M.S. Sanford, P.J.H. Scott, Copper-mediated radiofluorination of arylstannanes with [^{18}F]KF, Org. Lett. 18 (2016) 5440–5443, https://doi.org/10.1021/acs.orglett.6b02911.
[56] C. Hoffmann, N. Kolks, D. Smets, A. Haseloer, B. Gröner, E.A. Urusova, H. Endepols, F. Neumaier, U. Ruschewitz, A. Klein, B. Neumaier, B.D. Zlatopolskiy, Next generation copper mediators for the efficient production of ^{18}F-labeled aromatics, Chem. Eur J. 29 (2023) e202202965, https://doi.org/10.1002/chem.202202965.
[57] J. Zischler, N. Kolks, D. Modemann, B. Neumaier, B.D. Zlatopolskiy, Alcohol-enhanced Cu-mediated radiofluorination, Chem. Eur J. 23 (2017) 3251–3256, https://doi.org/10.1002/chem.201604633.
[58] A.M. Bernard, M.G. Cabiddu, S. De Montis, R. Mura, R. Pompei, Synthesis of new compounds with promising antiviral properties against group A and B Human Rhinoviruses, Bioorg. Med. Chem. 22 (2014) 4061–4066, https://doi.org/10.1016/j.bmc.2014.05.066.
[59] R.L. Hudkins, L.J.S. Knutsen, P.C. P, B.G. Sundar, K.J. Wells-Knecht, Substituted pyridazine derivatives which have histamine H3 antagonist activity, WO 2009/097306 A1. https://lens.org/106-000-855-446-766, 2009.
[60] D.R. Renk, M. Skraban, D. Bier, A. Schulze, E. Wabbals, F. Wedekind, F. Neumaier, B. Neumaier, M. Holschbach, Design, synthesis and biological evaluation of Tozadenant analogues as adenosine A$_{2A}$ receptor ligands, Eur. J. Med. Chem. 214 (2021) 113214, https://doi.org/10.1016/j.ejmech.2021.113214.
[61] E. Fiorica-Howells, R. Hen, J. Gingrich, Z. Li, M.D. Gershon, 5-HT$_{2A}$ receptors: location and functional analysis in intestines of wild-type and 5-HT$_{2A}$ knockout mice, Am. J. Physiol. Liver Physiol. 282 (2002) G877–G893, https://doi.org/10.1152/ajpgi.00435.2001.
[62] X. Li, K. Guo, T. Li, S. Ma, S. An, S. Wang, J. Di, S. He, J. Fu, 5-HT2 receptor mediates high-fat diet-induced hepatic steatosis and very low density lipoprotein overproduction in rats, Obes. Res. Clin. Pract. 12 (2018) 16–28, https://doi.org/10.1016/j.orcp.2016.03.015.
[63] E.T. Weber, R. Andrade, Htr2a gene and 5-HT$_{2A}$ receptor expression in the cerebral cortex studied using genetically modified mice, Front. Neurosci. (2010), https://doi.org/10.3389/fnins.2010.00036.
[64] M. Pompeiano, J.M. Palacios, G. Mengod, Distribution of the serotonin 5-HT$_2$ receptor family mRNAs: comparison between 5-HT$_{2A}$ and 5-HT$_{2C}$ receptors, Mol. Brain Res. 23 (1994) 163–178, https://doi.org/10.1016/0169-328X(94)90223-2.
[65] J.F. López-Giménez, G. Mengod, J.M. Palacios, M.T. Vilaró, Selective visualization of rat brain 5-HT$_{2A}$ receptors by autoradiography with [^{3}H]MDL 100,907, Naunyn-Schmiedeberg's Arch. Pharmacol. 356 (1997) 446–454, https://doi.org/10.1007/PL00005075.
[66] M.M. Bliziotes, A.J. Eshleman, X.-W. Zhang, K.M. Wiren, Neurotransmitter action in osteoblasts: expression of a functional system for serotonin receptor activation

and reuptake, Bone 29 (2001) 477–486, https://doi.org/10.1016/S8756-3282(01)00593-2.
[67] M. Bliziotes, A. Eshleman, B. Burt-Pichat, X.-W. Zhang, J. Hashimoto, K. Wiren, C. Chenu, Serotonin transporter and receptor expression in osteocytic MLO-Y4 cells, Bone 39 (2006) 1313–1321, https://doi.org/10.1016/j.bone.2006.06.009.
[68] B.I. Gustafsson, L. Thommesen, A.K. Stunes, K. Tommeras, I. Westbroek, H. L. Waldum, K. Slørdahl, M.V. Tamburstuen, J.E. Reseland, U. Syversen, Serotonin and fluoxetine modulate bone cell function in vitro, J. Cell. Biochem. 98 (2006) 139–151, https://doi.org/10.1002/jcb.20734.
[69] I. Westbroek, A. van der Plas, K.E. de Rooij, J. Klein-Nulend, P.J. Nijweide, Expression of serotonin receptors in bone, J. Biol. Chem. 276 (2001) 28961–28968, https://doi.org/10.1074/jbc.M101824200.
[70] D. Abramowski, M. Rigo, D. Duc, D. Hoyer, M. Staufenbiel, Localization of the 5-hydroxytryptamine$_{2C}$ receptor protein in human and rat brain using specific antisera, Neuropharmacology 34 (1995) 1635–1645, https://doi.org/10.1016/0028-3908(95)00138-7.
[71] J.M.F. Leysen, G.H.P. Van Daele, 4-Amino-N-(4-methyl-4-piperidinyl)-2-methoxybenzamides, 1994. WO 9402462.
[72] J.F. López-Giménez, L.H. Tecott, J.M. Palacios, G. Mengod, M.T. Vilaró, Serotonin 5-HT$_{2C}$ receptor knockout mice: autoradiographic analysis of multiple serotonin receptors, J. Neurosci. Res. 67 (2002) 69–85, https://doi.org/10.1002/jnr.10072.
[73] S.J. Finnema, V. Stepanov, A. Ettrup, R. Nakao, N. Amini, M. Svedberg, C. Lehmann, M. Hansen, G.M. Knudsen, C. Halldin, Characterization of [^{11}C]Cimbi-36 as an agonist PET radioligand for the 5-HT$_{2A}$ and 5-HT$_{2C}$ receptors in the nonhuman primate brain, Neuroimage 84 (2014) 342–353, https://doi.org/10.1016/j.neuroimage.2013.08.035.
[74] G.A. Kennett, M.D. Wood, F. Bright, B. Trail, G. Riley, V. Holland, K.Y. Avenell, T. Stean, N. Upton, S. Bromidge, I.T. Forbes, A.M. Brown, D.N. Middlemiss, T. P. Blackburn, SB 242084, a selective and brain penetrant 5-HT$_{2C}$ receptor antagonist, Neuropharmacology 36 (1997) 609–620, https://doi.org/10.1016/S0028-3908(97)00038-5.
[75] S.N. Andreassen, T.L. Toft-Bertelsen, J.H. Wardman, R. Villadsen, N. MacAulay, Transcriptional profiling of transport mechanisms and regulatory pathways in rat choroid plexus, Fluids Barriers CNS 19 (2022) 44, https://doi.org/10.1186/s12987-022-00335-x.
[76] V.V. Rao, J.L. Dahlheimer, M.E. Bardgett, A.Z. Snyder, R.A. Finch, A.C. Sartorelli, D. Piwnica-Worms, Choroid plexus epithelial expression of MDR1 P glycoprotein and multidrug resistance-associated protein contribute to the blood–cerebrospinal-fluid drug-permeability barrier, Proc. Natl. Acad. Sci. USA 96 (1999) 3900–3905, https://doi.org/10.1073/pnas.96.7.3900.
[77] N. Seneca, S.S. Zoghbi, J.-S. Liow, W. Kreisl, P. Herscovitch, K. Jenko, R. L. Gladding, A. Taku, V.W. Pike, R.B. Innis, Human brain imaging and radiation dosimetry of ^{11}C-*N*-Desmethyl-Loperamide, a PET radiotracer to measure the function of P-glycoprotein, J. Nucl. Med. 50 (2009) 807–813, https://doi.org/10.2967/jnumed.108.058453.
[78] J. Toyohara, M. Sakata, K. Ishibashi, P. Mossel, M. Imai, K. Wagatsuma, T. Tago, E. Imabayashi, N.A. Colabufo, G. Luurtsema, K. Ishii, First clinical assessment of [^{18}F]MC225, a novel fluorine-18 labelled PET tracer for measuring functional P-glycoprotein at the blood–brain barrier, Ann. Nucl. Med. 35 (2021) 1240–1252, https://doi.org/10.1007/s12149-021-01666-9.
[79] C. Hocke, S. Maschauer, H. Hübner, S. Löber, W. Utz, T. Kuwert, P. Gmeiner, O. Prante, A series of ^{18}F-labelled pyridinylphenyl amides as subtype-selective radioligands for the dopamine D3 receptor, ChemMedChem 5 (2010) 941–948, https://doi.org/10.1002/cmdc.201000067.
[80] A. Ettrup, S. da Cunha-Bang, B. McMahon, S. Lehel, A. Dyssegaard, A.W. Skibsted, L.M. Jørgensen, M. Hansen, A.O. Baandrup, S. Bache, C. Svarer, J.L. Kristensen, N. Gillings, J. Madsen, G.M. Knudsen, Serotonin 2A receptor agonist binding in the human brain with [^{11}C]Cimbi-36, J. Cerebr. Blood Flow Metabol. 34 (2014) 1188–1196, https://doi.org/10.1038/jcbfm.2014.68.
[81] H. Kubota, A. Kakefuda, T. Watanabe, N. Ishii, K. Wada, N. Masuda, S. Sakamoto, S. Tsukamoto, Synthesis and pharmacological evaluation of 1-Oxo-2-(3-piperidyl)-1,2,3,4- tetrahydroisoquinolines and related analogues as a new class of specific bradycardic agents possessing I_f channel inhibitory activity, J. Med. Chem. 46 (2003) 4728–4740, https://doi.org/10.1021/jm0301742.
[82] M.J. Adler, A.D. Hamilton, Oligophenylenaminones as scaffolds for α-helix mimicry, J. Org. Chem. 76 (2011) 7040–7047, https://doi.org/10.1021/jo200917d.
[83] Y. Su, J. Wang, R. Bao, Inhibitor Containing Bicyclic Derivative, Preparation Method Therefor and Use Thereof, EP 3971187 A1, 2020. https://lens.org/109-145-360-365-653.
[84] S. Humpert, C. Hoffmann, F. Neumaier, B.D. Zlatopolskiy, B. Neumaier, Validation of analytical HPLC with post-column injection as a method for rapid and precise quantification of radiochemical yields, J. Chromatogr. B 1228 (2023) 123847, https://doi.org/10.1016/j.jchromb.2023.123847.